PONTIFICIA UNIVERSIDAD CATÓLICA DEL PERÚ

ESCUELA DE POSGRADO

DESARROLLO Y COMPARACIÓN DE DIVERSOS MAPAS DE PROBABILIDADES EN 3D DEL CÁNCER DE PRÓSTATA A PARTIR DE IMÁGENES DE HISTOLOGÍA

By

Kristians E. Diaz Rojas

Thesis submitted in partial fulfillment of the requirements for the degree of

Master in Digital Signal and Image Processing

in the Graduate School of the Pontificia Universidad Católica del Perú.

Thesis Supervisor: Benjamín Castaneda Aphan, Ph.D.

Examining commitee members:

Paul A. Rodríguez Ph.D.

Roberto J. Lavarello Ph.D.

Lima, Perú

April, 2013

Abstract

Understanding the spatial distribution of prostate cancer and how it changes according to prostate specific antigen (PSA) values, Gleason score, and other clinical parameters may help comprehend the disease and increase the overall success rate of biopsies. This work aims to build 3D spatial distributions of prostate cancer and examine the extent and location of cancer as a function of independent clinical parameters. The border of the gland and cancerous regions from whole-mount histopathological images are used to reconstruct 3D models showing the localization of tumor. This process utilizes color segmentation and interpolation based on mathematical morphological distance. 58 glands are deformed into one prostate atlas using a combination of rigid, affine, and b-spline deformable registration techniques. Spatial distribution is developed by counting the number of occurrences in a given position in 3D space from each registered prostate cancer. Finally a difference between proportions is used to compare different spatial distributions. Results show that prostate cancer has a significant difference (SD) in the right zone of the prostate between populations with PSA greater and less than 5 ng/ml. Age does not have any impact in the spatial distribution of the disease. Positive and negative capsule-penetrated cases show a SD in the right posterior zone. There is SD in almost all the glands between cases with tumors larger and smaller than 10% of the whole prostate. A larger database is needed to improve the statistical validity of the test. Finally, information from whole-mount histopathological images could provide better insight into prostate cancer.

Contents

List of Figures

TESIS PUCP

LIST OF FIGURES

PONTIFICIA
UNIVERSIDAD
CATÓLICA
DEL PERÚ

IV

List of Tables

Chapter 1

Introduction

The prostate is a male sex gland about the size of a walnut located bellow the bladder (the organ that stores and releases urine) and in front of the rectum. The urethra, the tube that carries urine from the bladder, passes through the center of the prostate, as shown in Figure 1.1. The prostate is anatomically divided into three zones: peripheral, central and transitional. The peripheral zone comprises the majority of the prostatic volume (approximately 65%). The central zone is the second largest region in the prostate comprising approximately 25% of its volume. The transition zone consists of two lobes that surround the proximal urethral segment laterally and interiorly [4].

The primary function of the prostate is to secrete an alkaline fluid that constitutes part of the seminal fluid, which is responsible for carrying the sperm during ejaculation.

The prostate gland tends to increase in size with the years, which can cause the urethra to become narrower and decrease urine flow, causing pain on patients. Prostate diseases occur commonly in men over 40 years. Men who suffer from these diseases have urinary problems that affect their quality of life. The more common benign (non-cancerous) prostate problems are:

- **Benign Prostatic Hyperplasia (BPH)** - is the medical term for enlargement of the prostate gland, BPH is the most common non-cancerous prostate problem, occurring in most men by the time they reach their 60s. Symptoms are slow, interrupted, or weak urinary stream. Although it is not cancer, BPH symptoms are often similar to those of prostate cancer.

- **Prostatism** - the symptom of decreased urinary force due to obstruction of flow through the prostate gland. The most common cause of prostatism is BPH.

- **Prostatitis** - inflammation or infection of the prostate gland characterized by discomfort, pain, frequent or infrequent urination, and sometimes fever.

- **Prostatalgia** - pain in the prostate gland, also called prostatodynia. It is frequently a symptom of prostatitis.
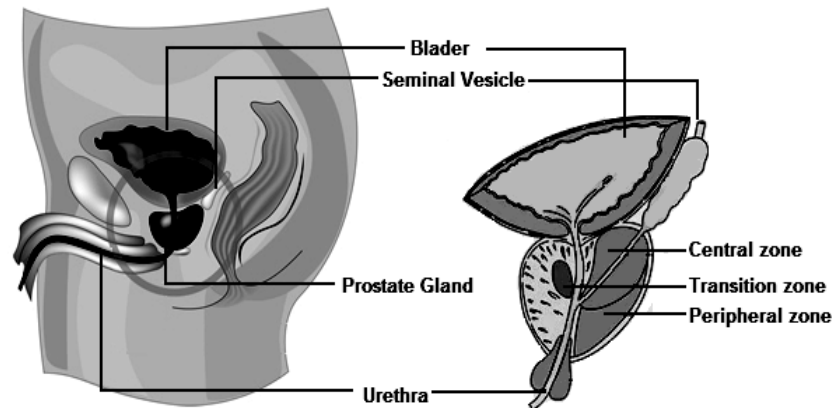
Figure 1.1: Anatomy of the prostate gland which is divided into peripheral, central and transitional zones. The prostate is located bellow the bladder and in front of the rectum.

The cancer occurs when some prostate cells mutate and begin to multiply uncontrollably. They may also spread from the prostate to other parts of the body, especially bones and lymph node causing metastasis [5].

According to the American Cancer Society the prostate adenocarcinoma remains a disease that affects most men. The estimated incidence and mortality numbers for 2012 due to this disease were 241,740 and 28,170 [3]. Prostate cancer is the second most common cancer among peruvian men [6]. Worldwide the incidence and mortality numbers are approximately 899,000 and 258,000, respectively. (Web: GLOBOCAN 2008, 2012 [7]).

1.1 Current Medical Procedure

The doctor inserts his finger into the rectum to examine the prostate. The doctor feels texture, shape or size of the gland in order to find tumors that may be in it. This test is called a digital rectal examination (DRE). A palpable abnormal nodule (lump or hard knot) and/or asymmetry may indicate prostate cancer. Although the DRE has a good positive predictive value [8], few tumors are detected only with an abnormal DRE [9]. A problem with the DRE is the low reproducibility of the results due to inter-observer variability [9]. The sensitivity of DRE is low: about 17% of men with a normal DRE are diagnosed with prostate cancer after a biopsy. Because of its low sensitivity, low specificity and high error rate associated with the sub-classification, digital rectal examination should not be used as the only screening method.

Prostate specific antigen (PSA) is a substance in the blood that is produced naturally by the prostate gland. High levels of PSA (greater than 4 ng/mL for Peru and the USA.) may be an indication of prostate infection, inflammation, enlargement or cancer.
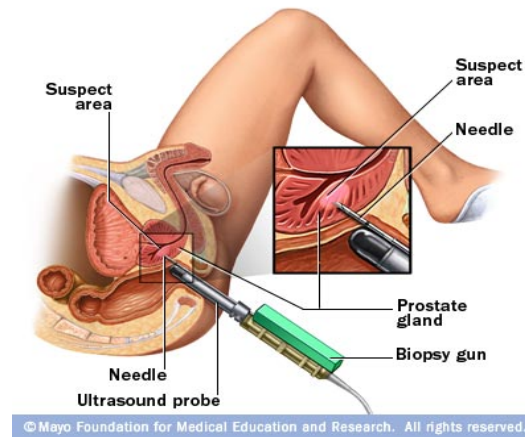
Figure 1.2: During a transrectal biopsy, a biopsy gun is inserted through the rectum and small sections of the prostate glands tissue are removed for analysis. The original image is from Mayo Foundation for Medical Education and Research [1].

PSA combined with DRE can help identify prostate cancer in its early stages. It is, however, necessary to perform a biopsy, which is guided by transrectal ultrasound imaging (TRUS), see Figure 1.2. TRUS is the preferred imaging modality over computed tomography (CT) and magnetic resonance imaging (MRI) mainly due to its non-invasive (does not modify the physical properties of tissue), non-ionizing, and low-cost characteristics. Other reason for using TRUS is its association with lesions as hypo-echoic nodules located in the periphery of the gland [10]. However, TRUS images have a low signal to noise ratio (SNR) and a low contrast; therefore biopsy examinations have a low level of success, the results depending on the empirical experience of the radiologist. Flaningas et al. [11] showed in their publication that biopsy tests usually have a success rate around 30% using the six-core biopsy protocol. Other studies indicate that to increase the level of success more cores should be taken directly affecting the patient.

It is for this reason that several researchers started building virtual 3D models of the prostate and simulating prostatic biopsy tests. Different biopsy schemes can be virtually simulated and evaluated before clinical application. The use of virtual 3D models or probabilistic maps (atlas) is is to the study the areas within the prostate gland where the cncer is more likely to develop. An estimation of the tumor distribution has a significant impact to both clinical and academic interests. In Table 1.1 it is summarized the different publications in prostate biopsy simulation [2].

Different researchers have begun to explore the possibility of using a large number of histological pictures to develop a probability map containing the tumor distribution within the prostate gland. This distribution map can be used to study the efficiency of existing biopsy schemes, or to design optimal biopsy strategies [16, 17, 18, 19, 20, 22, 33].

A key problem involved in this study is the registration of 3D surface models. All the studied prostate models need to be reshaped, so that tumors are placed in a uniform

Table 1.1: Published articles of computerized simulation of prostatic biopsy, the original table is from [2].

References	Description	Number of prostate
Bauer et al. [12]	Sextant (72.6%), 10-core and 12-core (99.0%), 14-core (99.5%), 5-region (12-core) (90.5%)	201
Bauer et al. [13, 14]	Sextant (54.3%), 5-reg (10-core) (100.0%)	35
Zeng et al. [15]	Sextant (71.5%), 10-core (96.4%), 12-core (97.2%), 5-reg (12-core) (89.7%)	281
Zeng et al. [16, 17]	Zone-based 3D distribution map of prostate cancer (8-division and 48-division schemes)	281
Shen et al. [18, 19]	Deformable registration. Atlas-based optimal biopsy strategy	64(of 281)
Opell et al. [20]	Zone-based 3D distribution map of prostate cancer (24-division scheme)	281
Sofer et al. [21]	Atlas-based optimal biopsy strategy (48-division scheme)	301
Shen et al. [22]	Deformable registration. Atlas-based optimal biopsy strategy	100
Zeng et al. [23]	Correlation between biopsy core volume and tumor volume	107
Chen et al. [24]	Sextant (73%), 10-core (96%). Tumor volume > 0.5 cm^3	180(607) [a]
Chen et al. [25]	Ten schemes including 5-reg (18-core) (87%), 11-core (94%), etc. Tumor volume > 0.5 cm^3	180
Chen et al. [26]	Sextant (18% when tumor volume < 0.5 cm^3, 73% when tumor volume > 0.5 cm^3)	180(607) [a]
Babaian et al. [27]	A 11-core multi-site directed biopsy (sextant plus 3 alternate sites)	183 + 179 [b]
Loch and Chen [28]	Computer simulation of prostate biopsy schemes	N/A
Daneshgari et al. [29]	Sextant scheme. Tumor volume < 6.0 cm^3	N/A
Crawford et al. [30]	Standard 6-core regarding different criterias of significance	59
Kawata et al. [31]	Systematic sextant biopsy and laterally directed 6-core biopsy	86 + 40b
Loughlin et al. [32]	Standard 6-core, 10-core (no results presented)	N/A
Frimmel et al. [33]	Spatial distribution of prostate tumours regarding tumour volume	81
Egevad et al. [34]	Impacts of position and direction of 10-core	75
Egevad et al. [35]	Evaluate the 3D prostate model, using simulation results of 10-core biopsy	81

[a] 607 tumour foci in 208 specimens.

[b] Data from two different institutions.

prostate. Some researchers used manual registration of 2D slices (Xuan et al. [36]). Frimmel et al. [33] dividing all prostate models into three groups by size (small, medium and large). Prostate models were reshaped into the shape of one of these three groups using a 2D reshaping algorithm. Shen et al. [18, 19, 22] presented the use of a deformation based registration approach using an adaptive focus deformable model (AFDM) [37, 38] to spatially normalize the external and internal structures of the prostate samples.

One of the problems with the registration task is the deformation process suffered by the prostate and the tumor. Zeng and coworkers [16, 17] investigated the spatial distribution of prostate cancer using a zone-based strategy, rather than deformation-based approaches. Prostate models were divided into 8 or 48 symmetric zones. First a quick 3D checking was performed to identify if a cancer is completely inside or outside a zone using the 3D bounding box, then a 2D scan line algorithm was applied to the 2D section planes to identify if the zone contained cancer. A similar work was proposed by Opell et al. [20], with the number of zones used equal to 24. However, the result of these works showed cancer distribution in a limited number of box zones (8-48) rather than anatomic zonal structures.

Frimmel et al. [33], and Shen et al. [18, 19, 22] showed that prostate cancer is mainly distributed along the periphery of the prostate. Zeng et al. [17] and Opell et al. [20] reported a significantly higher cancer distribution in the posterior zones than anterior zones.

However, these studies have focused on optimizing biopsy cores, without using other relevant information such as the PSA level of patients and their correlation with the location of tumor in the gland. Other parameters such as cancer volume and Gleason score (cancer grade descriptor) would have some impact on the tumor distribution [39]. Ou et al. proposed to evaluate the cancer significance and help improving the cancer volume estimation and Gleason Score, two of the most important surrogate markers. This is useful information for the treatment planning. It is for a better understanding of the disease, concerning its pathological variables, that the present research develops several probabilistic maps of the tumor distribution. Having this tool would help create a starting point for future works that would lead to a better understanding of the relationship between tumor distribution among different surrogate markers as PSA, Gleason Score, age, capsule penetration, etc.

For example, knowing whether prostate cancer for men under 60 has the same distribution as for men over 60 would allow different planning for each group. Both atlases would be analyzed statistically in order to determine if significant differences are found.

To develop the atlas, pathological and histological images will be used. The images were acquired using a digital camera and provided by University of Rochester, (Rochester, New York, U.S.A.). An expert radiologist made the segmentation of the tumor on histology images. We will use various topics of image processing for the creation of the atlas. After that we will carry out a statistical study of spatial distribution.

This thesis is distributed as follows: Chapter 2 describes the protocol of image acquisition and definitions of various markers used for selection of different atlas. Chapter 3 describes the methodology to develop the atlas. Chapter 4 describes the statistical method to differentiate spatial distribution. Results are presented in Chapter 5. Finally, Chapter 6 presents a brief discussion ending with discussion and conclusions.

Chapter 2

Gathering of Histopathological Data and Images

In order to accomplish the objectives of this research, it is important to build a database with information from patients that include histopathological variables, pathological and histological images and 3D reconstruction of the gland.

Histopathological variables are used to understand the spatial distribution of prostate cancer and how it changes according to clinical parameters in order to comprehend the disease. The color images from both, gross pathology and histological slices are used to build a 3D reconstruction of each patient's gland showing the location of the tumor. Then, with this information a registration algorithm is used to construct the spatial probability map. This process is presented in detail in Chapter 3.

Histopathological variables gathered for this thesis are: PSA value at time of the surgery, Gleason score, T-Stage, capsule penetration, age, percentage of cancer and volume of the gland.

The federal Health Insurance Portability and Accountability Act (HIPAA) training, information of the surrogate markers of patients and both pathology and histology images, were provided by University of Rochester Medical Center (URMC) at Rochester, New York, USA. An expert radiologist made the segmentation of the tumor on histology images using blue or black ink color markers.

2.1   Pathological Variables (Surrogate Marker)

2.1.1   Prostate-Specific Antigen (PSA)

The biological function of the prostate specific antigen is liquefying the seminal coagulum after ejaculation. It can be detected in the blood of all adult men. Elevated levels of PSA in blood serum are associated with benign prostatic hyperplasia and prostate cancer.

The effectiveness of PSA as a tumor marker has made a significant impact in the management of prostate adenocarcinoma. PSA was discovered in the 1970s, its application began in the 1980s, and its widespread usage began in the 1990s. in 1987, Stamey and co-workers were the first group to perform a clinical study showing the effectiveness of PSA as a tumor marker in prostate cancer [40].

PSA is secreted into seminal fluid at concentrations of $0.5-3$ ng/ml (i.e., about 1 million times more than those in plasma). In the USA and in Peru a cutoff level of 4 ng/ml has become widely used as a decision limit although it does not correspond to any reference value [41, 42, 43, 44].

The PSA concentrations in serum increase with age [45] and, therefore, the reference values are age-dependent. For example, in the USA, the level of 2.5 ng/ml is used in the age group $40-49$ years, 3.5 ng/ml at age $50-59$ years, 4.5 ng/ml at age $60-69$ years, and 6.5 ng/ml at age $70-79$ years [45]. The value of using age-specific reference ranges is debated. The probability of finding a prostate cancer in a man with a serum PSA of 4 ng/ml is about 20% and it is similar when PSA is in the range $2.6-4$ ng/ml [45]. So far there is no consensus on which cutoff to use for free PSA and it is furthermore dependent on the assay method.

2.1.2   Gleason Score

Donald F. Gleason introduced the Gleason grading system for prostate cancer used around the world. Gleason pattern or grading is a microscopic exam based on the glandular architecture which can be divided into five grades of growth, 5 belonging to the worst prognosis. The most prevalent and the second most prevalent patterns are graded and added to obtain a Gleason score [46] which ranges from 2 to 10. Gleason grades are shown as follows:

- Gleason grade 1, very well circumscribed and separate nodules. The glands are small, well-formed and approximately equal in size and shape.

- Gleason grade 2, the glands are less uniform in size, shape and have more tissue between them.

- Gleason grade 3, the glands vary in size and shape and are often angular. This is the most common pattern or grade.

- Gleason grade 4, fused, poorly defined glands. Many cells are invading the surrounding tissue.

- Gleason grade 5, the tissue does not have recognizable glands.

2.1.3   T-Stage

To select the treatment of a patient with prostate cancer, the most important marker is the T-Stage. If the biopsy confirms that cancer exists, more tests should be performed in order

to determine how far it has spread from within the prostate to nearby tissues or other body parts. This process is called staging.

Nowadays, there are two classification systems for clinical staging: the Whitmore-Jewett and the Tumor, Node, Metastases (TNM) classification systems. Whitmore introduced the first clinical staging classification system for prostate cancer in 1956, and Jewett modified it in 1975.

In URMC the classification system used is the TNM. This system was first adopted in 1975 by the American Joint Committee for Cancer Staging and End Results Reporting (AJCC). There are 4 Stages that describe the prostate cancer extension.

The TNM classification applies only to andenocarcinomas. This classification is summarized in Table 2.1.

The TNM system for describing the anatomical extent of the disease is divided in three components. T is used to describe the extent of primary tumor. N describes the absence or presence and extent of regional lymph node metastasis. M is used to describe the absence or presence of distant metastasis [3].

2.2 Database

Our database was comprised of information from patients including clinical parameters (PSA value at time of the surgery, Gleason score, T-Stage, capsule penetration, age, percentage of cancer and volume of the gland), images and 3D reconstructions of the glands.

58 patients consented to participate in this study. All the patients were scheduled to undergo a radical prostatectomy at the URMC, between 2007 and 2009. Their average age was 59.8 ± 5.47 years old ranging from 48.5 to 72.8 years old. Their mean PSA value at the time of surgery was 6.95 $ng/ml \pm 8.21$ ng/ml ranging from 1 ng/ml to 61.1 ng/ml. Their average Gleason score was 6.84 ± 0.71 ranging from 6 to 9. Their mean prostate weight was 51.8 $g\pm 11.9$ g ranging from $30g$ to $85g$. Their average cancer percentage was 20.71 cc ranging from $5cc$ to $60cc$.

In the federal Health Insurance Portability and Accountability Act (HIPAA) there are important regulations governing health insurance coverage protection and health information security for Americans and their families. The HIPAA training was taken in order to guarantee security and privacy of patient information.

Table 2.1: TNM Staging System, extracted from [3]

Primary Tumor (T)	
TX Primary tumor cannot be assessed	
T0 No evidence of primary tumor	
T1 Clinically in apparent tumor neither palpable nor visible by imaging	
T1a Tumor incidental histologic finding in $\leq$ 5 % of tissue resected	
T1b Tumor incidental histologic finding in > 5% of tissue resected	
T1c Tumor identified by needle biopsy (e.g., because of elevated PSA)	
T2 Tumor confi ned within prostate $^{\alpha}$	
T2a Tumor involves one half of a lobe or less	
T2b Tumor involves more than one half of lobe, but not both lobes	
T2c Tumor involves both lobes $^{\beta}$	
T3 Tumor extends through the prostate capsule	
T3a Unilateral extra capsular extension	
T3b Bilateral extra capsular extension	
T3c Tumor invades seminal vesicle(s)	
T4 Tumor is fi xed or invades adjacent structures other than seminal vesicles	
T4a Tumor invades bladder neck, external sphincter, or rectum	
T4b Tumor invades levator muscles or is fixed to pelvic wall, or both	
Regional Lymph Node (N)	
NX Regional lymph nodes cannot be assessed	
N0 No regional node	
N1 Metastasis in single lymph node, $\leq$ 2 cm	
N2 Metastasis in a single node, > 2 *cm* but $\leq$ 5 *cm*	
N3 Metastasis in a node >5 *cm*	
Distant Metastasis (M)	
MX Presence of metastasis cannot be assessed	
M0 No distant	
M1 Distant	
M1a Nonregional lymph node(s)	
M1b Metastasis in bone(s)	
M1c Metastasis in other site(s)	

$^{\alpha}$ Invasion into the prostatic apex or into (but not beyond) the prostatic capsule is not classified as T3, but as T2.

$^{\beta}$ Tumor found in one or both lobes by needle biopsy but not palpable or visible by imaging is classified T1c.
AUA, American Urological Association; PSA, prostate-specific antigen; TNM, tumor-node-metastasis.
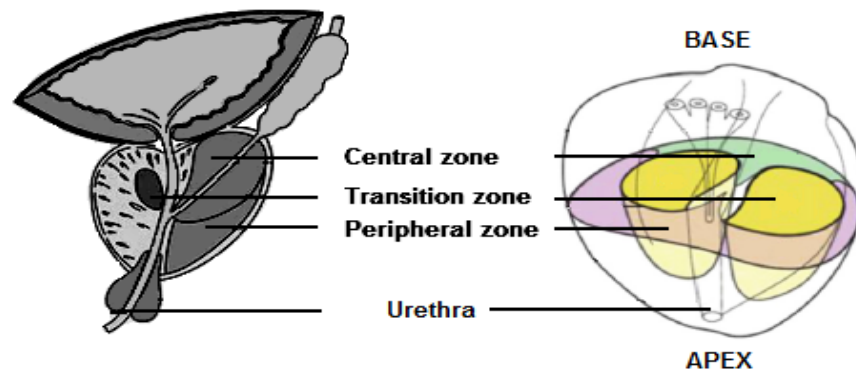
Figure 2.1: Anatomic description of the prostate, TZ: transition zone, PZ: peripheral zone, AFMS: anterior fibromuscular stroma. The original image is from [48].
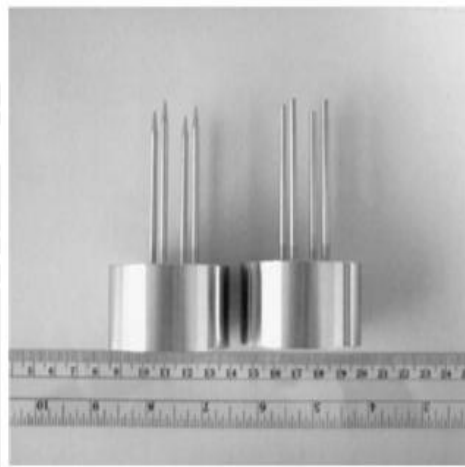
Figure 2.2: Device used as an external marker of the prostate, the devices was inserted in the specimen through the apex and the base parallel to the rectal surface of the prostate.The original image is from [49].

2.3 Image Acquisition Protocol

Prostate specimens were received after radical prostatectomy. Each gland was weighed and measured. These measurements include apex to base and anterior to posterior dimensions using calipers (see Figure 2.1 which describes the parts of the prostate), and gland volume. The gland was inked with different colors representing each quadrant using the CDI tissue marking dye system (Cancer Diagnostic Inc., Birmingham, MI). A device [47], which consists of two sets of four 3-*mm* diameter mating metal prongs (see Figure 2.2), was used to create markers for 3D reconstruction. Each set attached to a metal base in a square grid of 13*mm*. The prostate was inserted through the apex and the base symmetrically around the urethra. The specimen then was fixed in 4% formalin for 24 hours.

After fixation, the device was removed and the gland was measured again to assess the shrinkage factor. The prostate was then sectioned into 4 *mm* slices from the apex to the base. Depending on the size of the individual prostate, 6 to 12 gross pathology whole-mount slices (3 to 5 *mm* thick) were obtained. The processed whole-section slices were

embedded in Paraplast^{TM}, using large metal base molds (Surgipath Medical). Sections 45 μm thick were cut from the surface of each block. The slides were baked for 1 hour at $60°C$ and stained using routine hematoxilin-eosin protocol. The result was one histology slide for each gross slab. The microscope whole-mount sections were examined by an expert pathologist in order to recognize the tumor in every slice, and then the expert pathologist outlined the tumor using a marker ink blue or black.

Both gross pathology and histology slices were photographed after preparation, so that 3D reconstruction could be done. The color images both gross pathology and histological slices were captured using a digital camera (Diagnostic Spot RT digital color camera, Diagnostic Instruments Inc, Sterling Heights, MI). The sheets were mounted on a flat table, parallel to the focal plane of the camera. The distance between the camera and the sheets was about 30 cm. The images were stored on a computer using the Advanced Spot camera software (Diagnostic Instruments). For the gross specimens a caliper was used to measure the thickness of each slice. This measurement was used for 3D reconstruction.Additional information on the acquisition protocol is given in the article by Taylor et al. [49].

Chapter 3

3D Reconstruction of the Prostatic Gland (ATLAS)

The methodology followed to create the 3D spatial distribution consists of: first, alignment of the histological and pathological image of the same prostate; then segmentation the gland and the tumor in order to have the outlines; followed by interpolation to have an isotropic volume. For interpolation we use the distance between apex to base of the fresh gland when it is extracted, that information can be found on the patient info sheet, and finally one prostate is (selected as the atlas model) used as a reference and the other glands are warped against it (3D registration). The Figure 3.1 shows the block diagram of the methodology applied to build the 3D model.
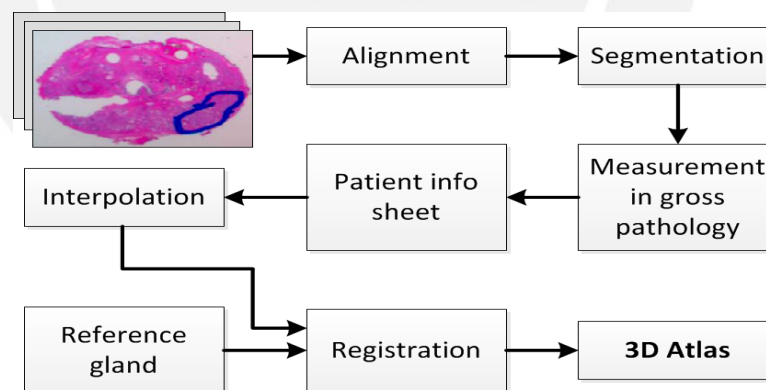
Figure 3.1: Methodology to build the 3D spatial distribution. First align the histological and pathological image of the same prostate; then segmentation the gland and the tumor; followed by interpolation to have an isotropic volume using the patient information sheet in order to get the distance between slices and finally the registration step.

3.1 Alignment

Since pathological and histological images are positioned differently during image acquisition, it is necessary to have an alignment step. First, all histological and pathological slices are registered to their respective central slices (fixed images) since they are more likely to
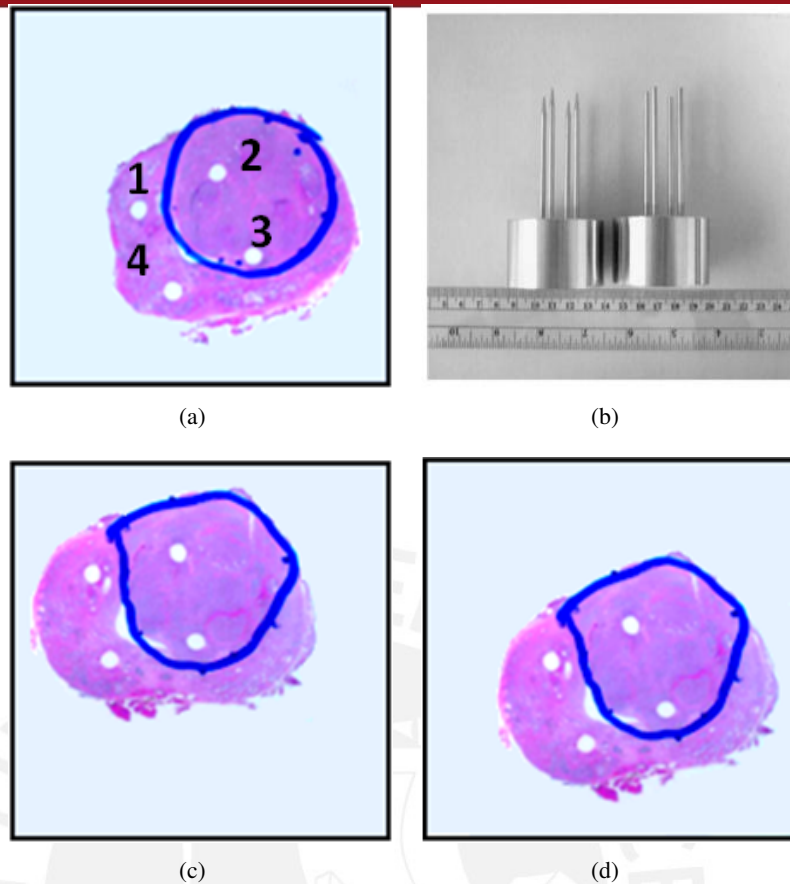
Figure 3.2: (a) Label of the four holes in the central histology slice. (b) Device used in the image acquisition protocol. (c) Next histological cut of the same prostate gland, It is not aligned with the base image (image a). (d) Result of image b align with the base image. The four holes in the prostate gland are used as landmarks in the alignment step.

show four holes caused by the marking device. Each hole is labeled clockwise with a number (see Figure 3.2a) in all slices. This step is performed manually.

The device used in the acquisition protocol provides landmarks which are 13 *mm* apart in a square configuration. This information is helpful to correct any deformations which the tissue underwent as part of the pathology processing. Figure 3.2a shows the four holes from the landmark device (Figure 3.2b) in a histology slice. Figure 3.2c shows the next slice from the same prostate. The holes are not positioned in the same place. Finally, Figure 3.2d shows the result after applying the alignment step to the second image.

There are two ways to warp an image [50]. The forward mapping scans through the source image, pixel by pixel, which copies them to the appropriate place in the destination image. The second, reverse mapping goes through the destination image, pixel by pixel, and samples the correct pixel from the source image. In the forward mapping case, some pixels in the destination might not get painted, and would have to be interpolated. So the reverse mapping is applied.
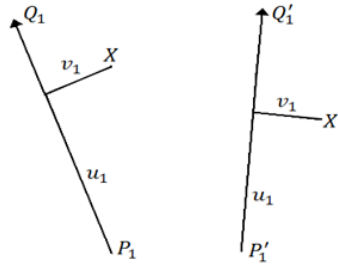
Figure 3.3: Single line pair

In the warping process, a pair of corresponding lines in the source and destination images define a coordinate mapping from the pixel X in the destination image to the pixel X' in the source image. Let's consider that the landmarks 1 and 4 form the line PQ in the destination image, similarly the landmarks 1 and 4 in the source image form the line $P'Q'$, as we can see in the Figure 3.3.

We calculate the distance of a pixel X to the line PQ obtaining v and the distance from P to the projection of X onto the line PQ obtaining u; with these values we determine the location of X' in the source image, maintaining the proportions. This procedure is repeated for all image points. The equations to calculate the new position are:;

$$u = \frac{\langle (X - P), (Q - P) \rangle}{\| Q - P \|^2} \tag{3.1}$$

$$v = \frac{(X - P) \perp (Q - P)}{\| Q - P \|} \tag{3.2}$$

$$X' = P' + u(Q' - P') + \frac{\langle v, Q' - P' \rangle}{\| Q' - P' \|} \tag{3.3}$$

Because there are four holes (four pairs of lines) a position X_i' is calculated for each pair of lines. The displacement $D_i = X_i' - X$ is the difference between the pixel location in the source and destination images, and a weighted average of those displacements is calculated (see Figure 3.4). Then a weight is assigned to each line which should be strongest when the pixel is exactly on the line, and weaker the further the pixel is away from it. For more detail see [51].

Due to the cutting and tearing in the acquisition protocol, some histological images will have missing parts (see Figure 3.5a). In order to determine a possible border, we propose to use information from its pathological counterpart. Following the same procedure to align the set of histology images, the holes in the corresponding pathology images are labeled and the warping transform is applied.

Pathology images are used when there is missing information in the boundary of the histological image (see next Section 3.2). In all cases the central slice of the prostate is selected as the fixed image, and the rest of the cuts are aligned to it.
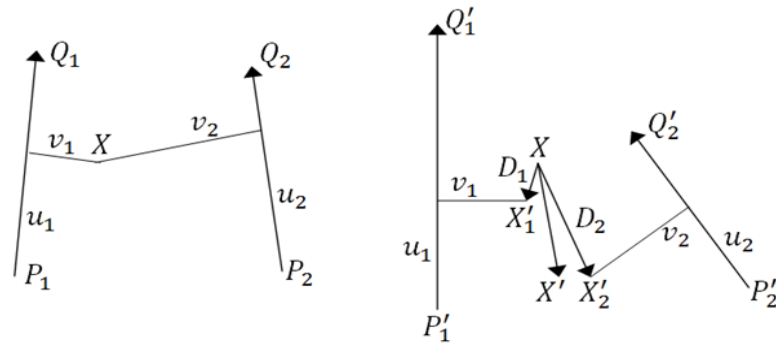
Figure 3.4: Multiples line pairs

Histological cuts of the base and apex do not always show all four holes. Since at least two holes are needed for the warping transformation, when only one hole is present a translation transform is applied.

3.2 Segmentation

The purpose of the segmentation is to identify the outline of the prostate and the shape of the tumor previously delimited by an expert pathologist. This segmentation step is required to generate a three-dimensional reconstruction of the prostate and the tumor.

Since the acquisition environment was not controlled when the digital images were taken, they have not been exposed to the same lighting conditions producing unwanted shadows and reflections. Therefore, a pre-processing step is required. The histological images have a characteristic red to pink color with a white background. Thus, the intensity levels corresponding to the image are located on the first mode of its histogram. The other mode corresponds to the background (highest intensity values - near white). The histogram is formed as the sum of each histograms layer. We detect the peak of the first mount to establish an upper threshold, whereas the lower threshold is established at the 10% intensity of the peak as seen in Figure 3.6. Finally, an image stretching transformation [52] is applied with these two thresholds.

After applying the pre-processing step to the histological images, they show a high contrast between the prostate and the background, as seen in the Figure 3.6c. The information of the prostate gland is located in the red and blue layers; therefore, the segmentation is obtained using the threshold t for both layers applying the following equation:

$$BW = \begin{cases} 1, I_r > t \text{ and } I_b > t \\ 0, \text{ otherwise} \end{cases} \tag{3.4}$$

Where I_r and I_b correspond to the red and blue layers of the histological image after

TESIS PUCP

CHAPTER 3. 3D RECONSTRUCTION OF THE PROSTATIC GLAND (ATLAS) 17

PONTIFICIA
UNIVERSIDAD
CATÓLICA
DEL PERÚ

(a)

(b)

(c)
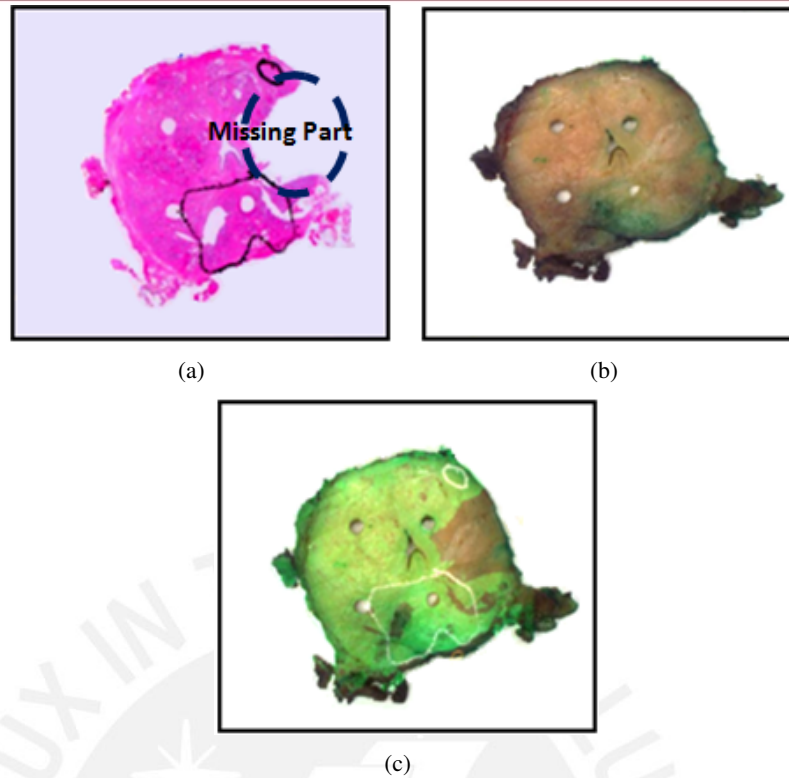
Figure 3.5: (a) The circle in dark blue in the histological image shows the missing boundary, the black outline is the localization of the cancer, this task is developed by an expert pathologist. (b) The counterpart gross pathology image of the image a. (c) Gross image alignment to the histological image, in green the overlay histological.

(a)

(b)

(c)
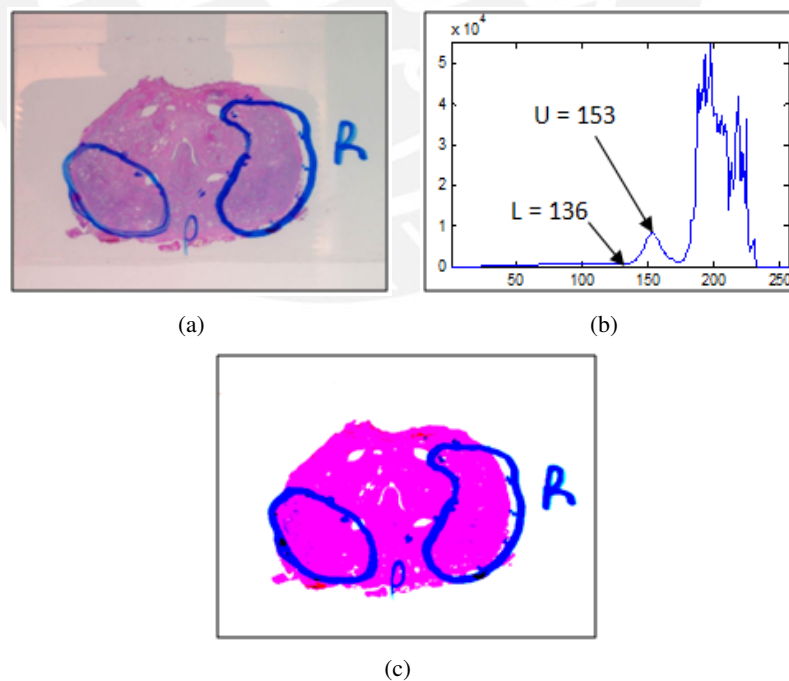
Figure 3.6: (a) Histological cut. The image shows the outline of the tumor and the label R (right of the patient) also shows unwanted shadows and reflections. (b) Image's histogram where L and U are the lower and upper threshold used to stretch the image. (c) Result to apply stretching transformation to the image a using U and L as limit threshold.

pre-processing respectively. The threshold value t is not critical since we can select it in a wide range (150 to 255) with the same result. We set the value to 200. Finally, mathematical morphology is applied to fill all the possible holes.

The tumor was delineated by an expert pathologist on the histology cut using a blue or black marker. To segment it from the image, an automated Otsu-based thresholding algorithm [53] was performed on the red layer. After this step, we only consider the objects which are within the previously segmented prostate.

Some histological images had missing parts (see Figure 3.5a). We propose to use information from its pathological counterpart to correct the segmented boundary [54].

To do this, we develop a semi-automatic algorithm. First, the pathological and histological images are aligned as explained in Section 2.2.1 (Figure 3.5c). Then the border of the segmented prostate is decomposed into a set of vertices, which are overlaid on the pathology image. A few vertexes are dragged on the desired boundary (pathology image) by the user.

Then Discrete Dynamic Contours (DDC) [55] are applied to move the rest of the outline closer to the correct boundary. The vertices inserted by the user (two or three) are clamped, this produces that adjacent vertices generally deform towards the clamped vertices. The contour is deformed by moving each of these vertices through a series of iterations according to the following kinematic equations:

$$P_i(t + \Delta t) = p_i(t) + v_i(t)\Delta t \tag{3.5}$$

$$v_i(t + \Delta t) = v_i(t) + a_i(t)\Delta t \tag{3.6}$$

$$a_i(t + \Delta t) = \frac{1}{m_i} f_i(t + \Delta t) \tag{3.7}$$

Where $p_i = (x_i, y_i)^T$ is the position of the vertex i; $v_i(t)$ and $a_i(t)$ are its velocity and acceleration, respectively; m_i is its mass which is assumed to be 1; and $t + \Delta t$ represent the time of the next iteration. The initial velocity and acceleration are set to zero.

The force f_i is the result of the sum of three terms:

$$f_i = w_i^{int} f_i^{int} + w_i^{img} f_i^{img} + f_i^d \tag{3.8}$$

Where f_i^{int}, f_i^{img} and f_i^d are the internal, image and damping forces, respectively; w_i^{int} and w_i^{img} are the weight which determine the contribution of each force.

The image forces are determined by

$$E(x^p, y^p) = \| \Delta(G_\sigma I(x^p, y^p)) \| \tag{3.9}$$

TESIS PUCP

CHAPTER 3. 3D RECONSTRUCTION OF THE PROSTATIC GLAND (ATLAS) 19

PONTIFICIA
UNIVERSIDAD
CATÓLICA
DEL PERÚ

$$f_i^{img}(x^p, y^p) = \frac{2\Delta E(x^p, y^p)}{max \parallel \Delta(E(x^p, y^p)) \parallel} \tag{3.10}$$

Where $E(x^p, y^p)$ represents the energy associated with a pixel in the image having coordinates (x, y), G_σ is a Gaussian smoothing filter, and I is the image.

The internal force is determined by

$$f_i^{int} = (\langle c_i, r_i \rangle - \frac{1}{2}(\langle c_{i-1}, r_{i-1} \rangle + \langle c_{i+1}, r_{i+1} \rangle))r_i \tag{3.11}$$

$$c_i = d_i - d_{i-1} \tag{3.12}$$

$$t_i = \frac{d_i + d_{i-1}}{\parallel d_i + d_{i-1} \parallel} \tag{3.13}$$

$$r_i = \begin{bmatrix} 0 & 1 \\ -1 & 0 \end{bmatrix} t_i \tag{3.14}$$

Where d_i is the unit edge vector from vertex i to vertex $i + 1$ and t_i is tangential unit vector associated with the vertex V_i.

The damping force is proportional to the velocity v_i at the vertex. $f_i^d = -0.5v_i$

We develop a semi-automatic algorithm. First, the pathological and histological images are aligned as explained in Section 2.2.1 (Figure 3.5c). Then the border of the segmented is decomposed into a set of vertices, which are overlaid on pathology image. A few vertexes are dragged on the desired boundary (pathology image) by the user.

This algorithm proposes is semi-automatic, therefore it is always subjective however DDC makes it easier the segmentation and edit it. In our experiments, the weights are $w_i^{int} = 0.6$ and $w_i^{img} = 0.4$. The image force is responsible of moving the vertex to the nearest and strongest edge as long as it is within the influence area which is determined by a two-dimensional Gaussian function. Internal forces are computed based on neighboring vertices and constrain the vertex to form a smooth contour. The damping force provides stability in the iteration process.

In addition to this problem, in some images, the pathologist did not completely delineate the tumor with a continuous solid line but with spaced dots (Figure 3.7a). To obtain the complete outline, cubic interpolation was applied (Figure 3.7b).

3.3   Measurement in Gross Pathology

To build the three-dimensional reconstruction of the prostate gland, it is necessary to quantify the separation between histology and gross pathology slices. The thickness of each gross pathology slab is measured using a caliper. Eight measurements are performed, two

TESIS PUCP

CHAPTER 3. 3D RECONSTRUCTION OF THE PROSTATIC GLAND (ATLAS) 20

PONTIFICIA
UNIVERSIDAD
CATÓLICA
DEL PERÚ

(a)   (b)
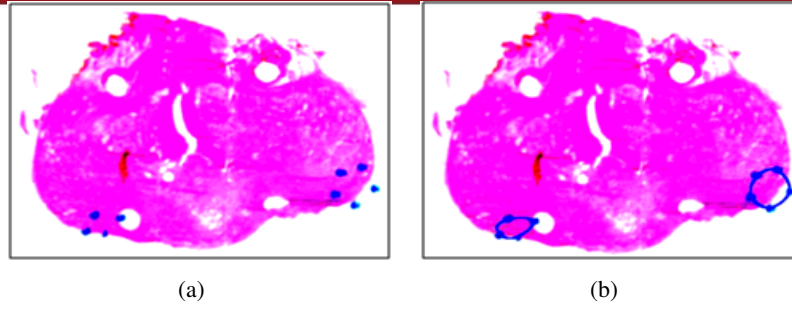
Figure 3.7: (a) The outline of the tumor was done using spaced dots. (b) Cubic interpolation was applied in order to obtain the complete outline.

Table 3.1: Measurement of Gross Pathology (mm)
AL: Apex Left, AR: Apex Right, PL: Posterior Left, PR: Posterior Right.

	Pearson 1				**Person 2**			
Slice	AR	AL	PR	PL	AR	AL	PR	PL
Method 1 - Inside	3.4	2.7	3.2	3.3	2.4	1.9	1.6	2.4
Method 2 - Outside	2.3	2.3	3.1	2.1	3.2	3.6	2.5	3.0

measurements per hole (one using the outside jaws and the other using the depth probe of the caliper, see Figure 3.8). This task is repeated by two observers and the average measure is utilized.

Table 3.1 shows the measurements obtained using both methods - outside jaws and the depth probe of the caliper, all the measures are in millimeters, the average is obtain for all readings to reduce measurement error. The result will be the distance between histology cuts.

The gland is subject to various handling during the acquisition process causing it to shrink or deformed, that is why one of the measurements taken when the prostate is removed is the distance between the apex and the base of the gland. This information is available in the patient information sheet and it was contrasted with the total distance ob-
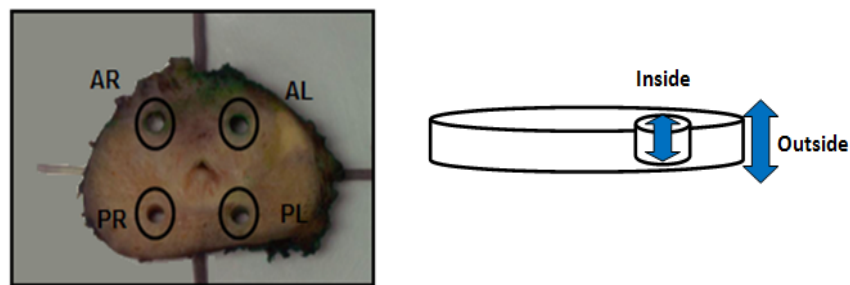
Figure 3.8: Measure internal and external by the use of the outside jaws and the depth probe in each holes, where AL: Apex Left, AR: Apex Right, PL: Posterior Left, PR: Posterior Right.

tained after the measurements using the caliper. Therefore, thickness values are scaled to make the sum of the thickness of all slices equal to the apex-to-base distance measured in the fresh prostate. Then, an interpolation step is required in order to have a coherent 3D reconstruction.

3.4 Interpolation

The distance between adjacent image elements (pixels) within a slice is smaller than the distance between adjacent image elements in two neighboring slices. Histology images have a thickness of 5 *μm* and are separated by 4 *mm*. Therefore, there are 8 frames by patient on average. In such situations, it is necessary to interpolate additional slices in order to obtain an isotropic volume.

There are several approaches for reconstructing and displaying 3D objects from serial cross sections [56], [57], [58]. The major difference of these approaches lies in the interpolation method employed. The two main categories of interpolation techniques for reconstructing objects are: grey-level and shape-based interpolations. Grey-level interpolation methods employ nearest-neighbor, linear or polynomial and splines interpolation. On the other hand, shape-based interpolation methods consider shape features extracted from the image. Shape-based interpolation converts binary images into distance maps using distance transformation functions such as Manhattan or city-block distance template [59, 60, 61] to approximate the Euclidean distance between the pixel and the contour of the object. Shape based interpolation is quite simple to understand, easy to implement and computationally fast. However, this method fails to interpolate slices when there is no overlapping area between the two objects.

For example, the Figure 3.9 shows the initial (Figure 3.9a) and last position (Figure 3.9e) of one object (there is not overlapping area between them) and three images added as result of apply Shape-based interpolation. We can observer that the central image (figure 3.9c) will not have any information of the object. Giving the impression that there are two objects, not one.

We used the method proposed by Lee and Wang [62] to overcome this limitation. A morphology-based interpolation method uses dilation and erosion morphological operators to create distance maps and perform the interpolation.

Before interpolation, it is necessary to align the objects (prostate slices) using their centroids. Then, for two aligned objects, there will be three possible regions, as seen in the Figure 3.10. We apply a dilation operator to regions I and II which represent the morphological difference between the two objects. The purpose of this step is to obtain the dilation-based distance to the boundary of region III (intersection of the two objects). After

(a)	(b)	(c)	(d)	(e)
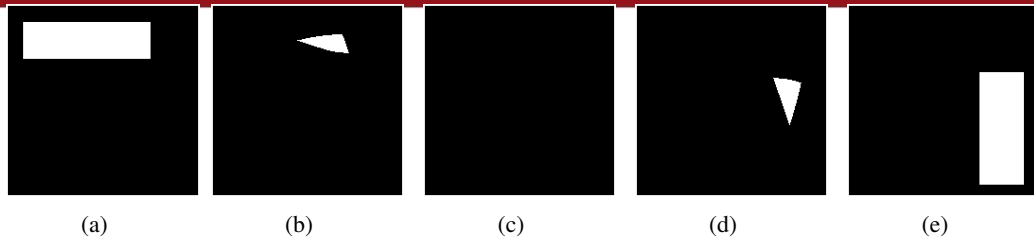
Figure 3.9: Result of applying shape based interpolation between (b) and (e) , both images have not overlapping area between them, given the impression that there are two objects: (a) - (b) and (d)-(e).
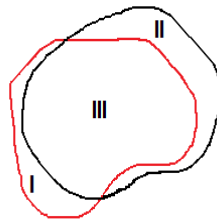
Figure 3.10: The region I and II are the morphologic difference between two objects after centralization. Color red object one, color black object two.

this, we can apply an erosion operator to interpolate the results. During interpolation, each pixel in both regions I and II will gradually move toward region III. For more detail of the kernel used in the dilation and erosion operators, the reader is directed to [62].

After interpolating the prostate, the same procedure is repeated for each tumor present in the gland. However, there are additional considerations to be taken in order to avoid ambiguities in the reconstruction. For example, Figure 3.11a, 3.11b and 3.11c shows the location of tumor in three slices, and in the Figure 3.11d and 3.11e their possible three-dimensional reconstruction. As we can see there is more than one option, since the tumor can grow in any direction and sense.

The first consideration is to determine tumor matching between slices since multiple cancers may exist on two input slices, for that purpose if the distance between the contours of the tumor was less than 5 *mm* then they correspond to the same cancer. This a heuristic based on the experience of the specialist. [63, 64].

The other decision rule is to create a pseudo-cancer by setting a small region in between two slides, one slide with tumor presence, and the other without it (Figure 3.12a). The pseudo-cancer is the resulting area of applying morphology erosion to the image right before there is no presence of tumor (Figure 3.12b).

We perform cancer-to-cancer interpolation and prostate-to-prostate interpolation, in separate steps. Finally, it is necessary to compensate the effects of centralization by trans-

(a)　　　　　　　　(b)　　　　　　　　(c)

(d)　　　　　　　　　　　(e)
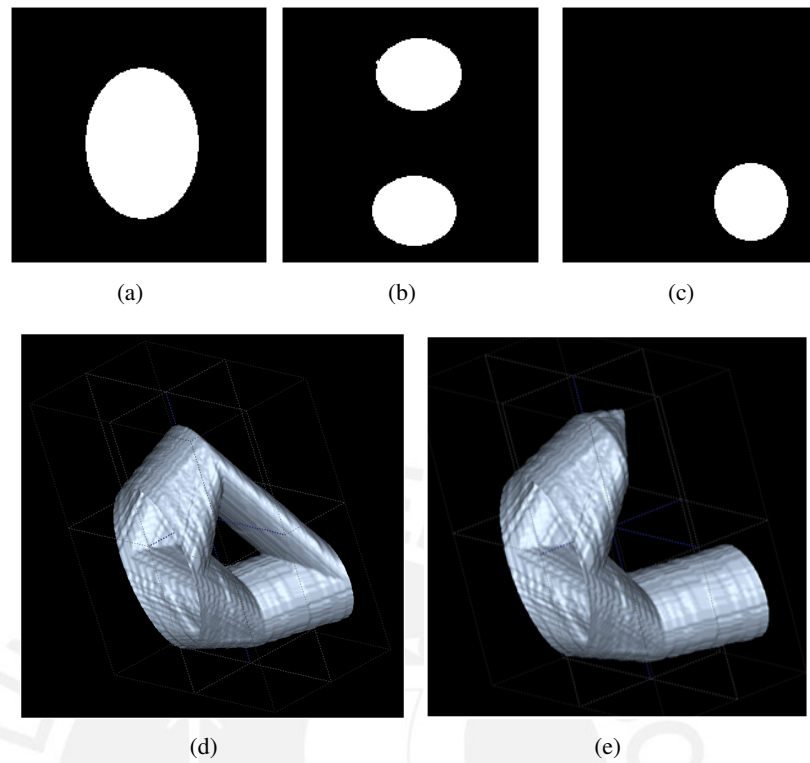
Figure 3.11: (a), (b) and (c) show the location of tumor in three consecutive slices, if there is not a rule of decision, there will be two possible 3D reconstruction (d) and (e).

(a)　　　　　　　　　　　(b)
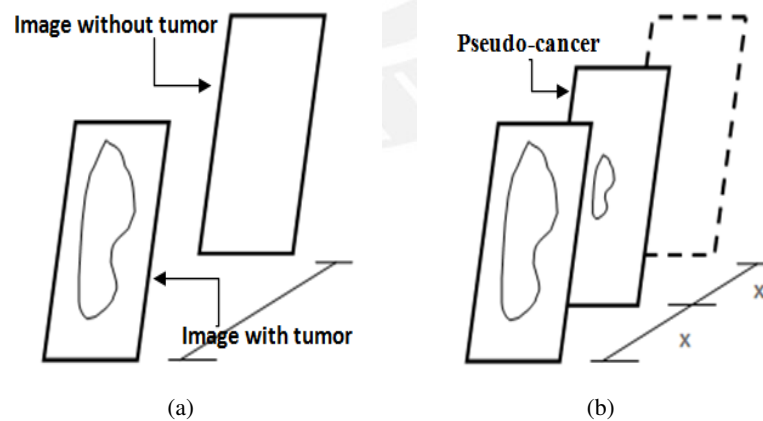
Figure 3.12: Since the thickness of the gross pathology images ($4-5$ *mm*) the tumor ends are not displayed. (a) Shows the tumor in one slice, in the next slice this information is missing. To make the 3D reconstruction, we insert a pseudo-cancer in between two slides, as show in (b) . The pseudo-cancer is the resulting area of applying morphology erosion to the image right before there is no presence of tumor.
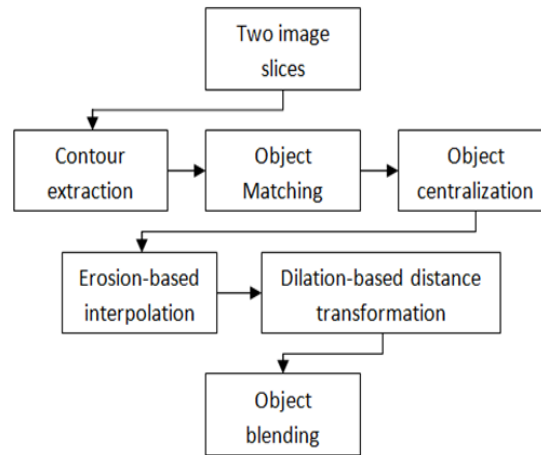
Figure 3.13: Block Diagram of the Morphology-Based Interpolation.

lating the interpolated object back to the correct position, computing the new centroid. Morphology-based interpolation can be schematized as shown in Figure 3.13.

Figure 3.14 shows the result obtained applying morphology based interpolation to the prostate gland and tumor. In the first row there are two histological prostate cuts, a physician expert outlined the tumor with a black marker ink. The first and last column of the second and last row show the segmented images of the gland and tumor segmentation respectively, between them we have added two slices by interpolation as described above. Each tumor matched is represented with a different color which indicates that it is the same tumor.

3.5 Registration

The registration process is composed of four steps. 1) A rigid registration is used to align the volumes. 2) An affine transformation allows compensation for shear and scale. 3) A deformable Bspline registration [65] with a coarse grid is applied and 4) Another Bspline registration with a finer grid. Rigid and affine transformations bring the registration process close to its global minimum, and B-spline transformations are used to compensate for deformations in the gland due to mechanical and chemical procedures in the histological processing. This approach is evaluated in [66].

Since our database is formed by whole prostatectomy gland subsequent to diagnosing of cancer; we do not have a healthy prostate and set as a model for the development of the atlas. Therefore, one prostate with average size and shape is selected manually to be the atlas model and the 3D reconstructions of the other glands are warped against it.
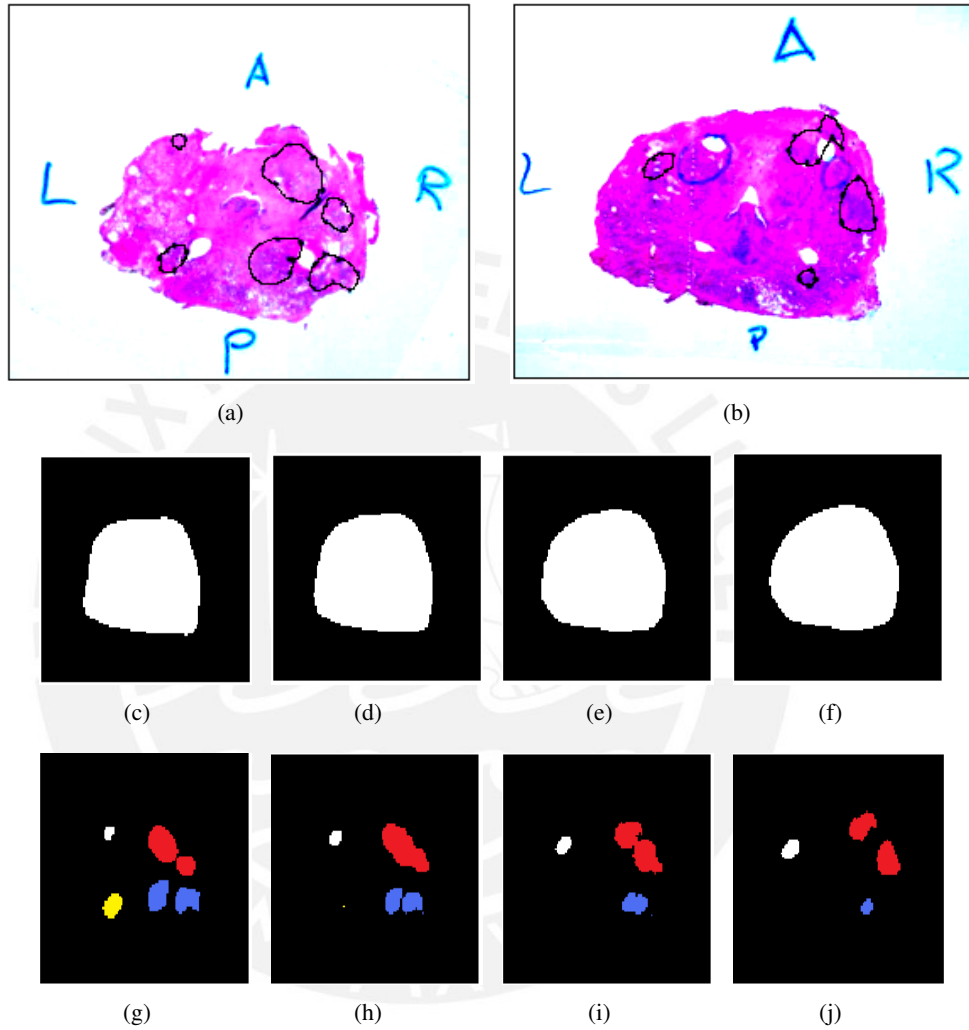
Figure 3.14: (a) and (b) corresponding to a histological prostate cuts which shown the location of the tumor in black color (outline by a pathologist); (c) and (f) shows the gland segmentation of histological images (a) and (b) respectively; (d) and (e) are the result of interpolation, added two slices between them; (g) and (j) shows the tumors segmentation of the images (a) and (b) respectively; (h) and (i) show the tumor interpolation. Each color indicates the same tumor.

Chapter 4

Statistical Analysis

Once all the prostate glands have been registered into a unique atlas model, the spatial distribution is developed by counting the number of occurrences in a given position in 3D space from each registered prostate reconstruction.

A group of medical specialists in the field, determined to perform the analysis to the following spatial distributions:

- PSA at the time of the surgery less than and greater than or equal to 4 ng/ml.

- Age less than and greater than or equal to 60 years old.

- Capsule penetration positive against negative.

- Gleason score equal to 6 against over than 6, and tumors larger and smaller than 10% of the whole prostate.

The effectiveness of PSA as a tumor marker has made a significant impact in management prostate adenocarcinoma. In the USA and Peru a cutoff level of 4 ng/ml has become widely used as a decision limit although it does not correspond to any reference value.

Prostate cancer is a slow-spreading disease, so the diagnosis of this disease usually occurs in men over 40 years, this cutoff level is suggested for early detection [45], men older than 60 years usually show an advanced disease, however an interesting point of analysis is to determine whether there is any particular distribution to men under this threshold, since people with this disease have shown more aggressive cancer compared to over 60 years.

The Gleason score of 6 is the most typical score. Gleason score greater than 6 indicates that prostate cancer is detected at later stages; understanding the spread of disease or the areas where it is more aggressive could give a better understand of this disease.

Capsule penetration indicates if the cancer is contained by the capsule that surrounds the prostate (negative capsule penetration), or if it has spread outside the gland (positive capsule penetration). Identify region of the prostate with significant difference between

TESIS PUCP

CHAPTER 4. STATISTICAL ANALYSIS

PONTIFICIA
UNIVERSIDAD
CATÓLICA
DEL PERÚ

27

Table 4.1: Inferential Statistical Test

Number of samples	Hypothesis evaluated	Test
Interval/Ratio Data		
Single sample	Hypothesis about a population mean	• The single-sample z test (σ known) • The single-sample t test (σ unknown)
	Hypothesis about a population parameter/characteristic other than the mean	• The single-sample chi-square test for a population variance
Two independent samples	Hypothesis about difference between two independent population means	• The t test for two independent samples • The z test for two independent samples
Ordinal/Rank-Order Data		
Single sample	Hypothesis about a population median or the distribution of data in a single population	• The Wilcoxon signed-ranks test • The Kolmogorov Smirnov goodness-of-fit test for a single sample
Two independent samples	Hypothesis about two independent population medians, or some other characteristic of two independent populations	• The Mann Whitney U test • The Kolmogorov Smirnov test for two independent Samples
Categorical/Nominal Data		
Single sample	Hypothesis about distribution of data in a single population	• The chi-square goodness-of-fit test • The z test for a population proportion • The chi-square test of independence
Two independent samples	Hypothesis about distribution of data in two independent populations	• The chi-square test for homogeneity • The Fisher exact test • The z test for two independent proportions
Two independent samples	Hypothesis about distribution of data in two dependent populations	• The McNemar test

positive and negative capsule penetration will be useful to understand the disease and have an appropriate treatment.

Table 4.1 shows the most common statistical tests used [67]. To select the appropriate inferential statistical test, the following protocol is followed.

1. State the general hypothesis that is being evaluated.

2. Determine if the study involves a single sample or more than one sample.

3. If there is more than one sample, determine how many samples there are and whether they are independent or dependent.

4. Determine the level of measurement represented by the data that are being evaluated (which represents the dependent variable in the study). The level of measurements is: interval/ratio or ordinal/rank-order or categorical/nominal.

We propose to use the Z-test [67] for subgroup pairs to analyze differences distribution between two populations where each population has a common pathological variable. The Z-test for two independent proportions is most commonly employed to evaluate the null and

alternative hypotheses that are described for the Fisher exact test.

The use of Z-test for two independent proportions is valid since we want to evaluate the hypothesis about distribution of data in two independent populations which are assumed to have normal distribution [67]. The alternative hypothesis is that proportions are different, this is a non-directional alternative hypothesis, and it is evaluated with a two-tailed test.

Null Hypothesis :

$$H_0 : \pi_1 = \pi_2 \tag{4.1}$$

where π_1 and π_2 are the population proportion 1 and 2 respectively.

Alternative hypotheses :

$$H_0 : \pi_1 \neq \pi_2 \tag{4.2}$$

The following equation is employed to calculate the test static

$$Z = \frac{(p_1 - p_2) - (\pi_1 - \pi_2)}{\sqrt{\frac{p_1(1-p_1)}{n_1} + \frac{p_2(1-p_2)}{n_2}}} \tag{4.3}$$

Where:

- n_1 represents the number of persons in one of the populations.

- n_2 represents the number of persons in the other populations.

- p_1 represents the proportion of the first population, It is employed to estimate the population proportion π_1

- p_2 represents the proportion of the second population, It is employed to estimate the population proportion π_2

The proportions are defined as the number of occurrences divided by total number of patients that correspond to the population of study and analysis (e.g., fifty-eight if we analyze the entire population, see Figure 4.1).

The difference between proportions is applied to each voxel and is evaluated with a Z-test in order to ensure that the voxel is significantly different between the two spatial distributions; this process is repeated for all the voxels corresponding to the prostate atlas model. We use the critical Z value for two tails 1.65 (equivalent to $p = 0.1$) in order to find significant difference (SD).

Table 4.2 shows the number of patients by pathological variable using the threshold suggested by the physician. In the case of Gleason score, there are not enough patients in the group where Gleason score = 6 to perform a valid statistical evaluation. Similarly with PSA lest than 4 ng/ml.

(a) Patient 1   (b) Patient 2

(c) Spatial distribution
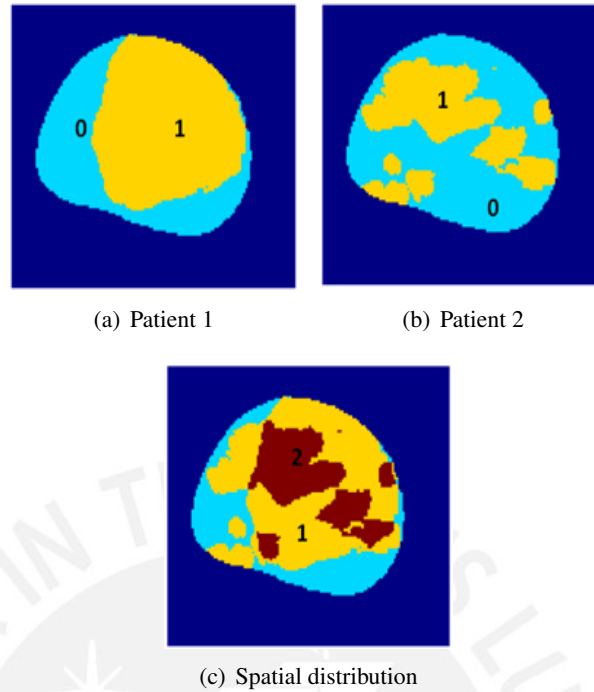
Figure 4.1: Spatial distribution employing two patients; for each patient the color yellow and cyan represents the zones with and without tumor, respectively. The value of one and zero is assigned to the yellow and cyan zone, respectively. To generate the spatial distribution we count the number of occurrence after sum the two images. The color red corresponds to two occurrences.

Table 4.2: Number of patients by pathological variable using the threshold suggested by physician

		Number of patients
PSA	$> 4ng/ml$	44
	$\leq 4ng/ml$	14
Gleason score	$= 6$	15
	$\neq 6$	43
Age	> 60 years old	35
	$\neq$ 60 years old	25
Capsule penetration	Positive	24
	Negative	34
Tumors size	> 10% of the whole prostate	28
	$\neq$ 10% of the whole prostate	30

Table 4.3: Final subgroup by pathological variable used in this thesis

		Number of patients
PSA	$> 5 ng/ml$	29
	$\leq 5 ng/ml$	29
Age	> 60 years old	35
	$\neq$ 60 years old	25
Capsule penetration	Positive	24
	Negative	34
Tumors size	> 10% of the whole prostate	28
	$\neq$ 10% of the whole prostate	30

Table 4.3 shows the number of patients by pathological variable with the threshold used in this research.

The values chosen as threshold in each parameter is compromise between commonly accepted clinical thresholds separating high and low values, and the number of patients in each subgroup required to make a good statistical evaluation.

The value used for PSA analysis is 5 ng/ml; in order to obtain representative statistical analysis (both populations of 29 patients). There is no report in the literature about the exact cutoff values for PSA.

Another statistical analysis is performed to obtain a better idea of significant difference by region and not global, for that we divided the prostate into a grid of 12 zones that are identifiable and accessible by physician (urologist). The grid has three transverse layers along the (patient's) vertical axis: base, middle and apex. Each layer is divided into two coronal layers from the rear to the front, denoted by posterior and anterior. Finally the layers are divided from left to right into 2 sagittal layers, left and right (see Figure 4.2).

Figure 4.2: A prostate models with 12 zones division, and his three views

Chapter 5

Results

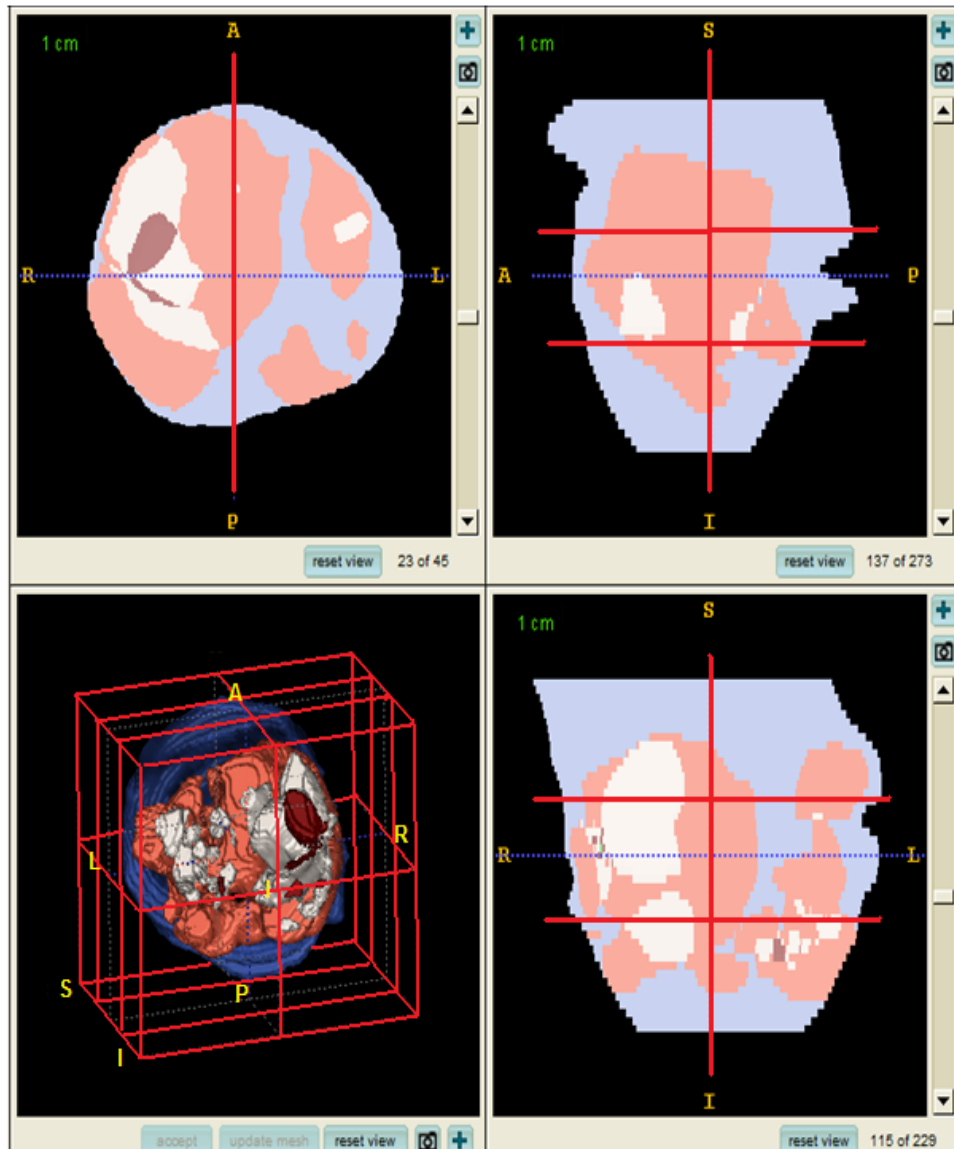The database consist of 58 prostates gland and the PSA information, capsule penetration, patient age, and percentage of cancer. Figure 5.1 shows the cancer probability distribution of the complete database. The result shows that the prostate cancer is more likely to occur in the right zone of the prostate. We used a color map in order to facility the zones with more level of occurrences, the color scale indicates the number of occurrences for a given population.

Statistical analysis shows that for population with PSA greater and less than 5 ng/ml, they have the spatial significant difference (SD) in the right zone of the prostate. Figure 5.2 shows the two spatial distributions and their SD. Similar results for population with positive and negative capsule penetration were obtained (Figure 5.4). In the case of populations older and younger than 60 years old, Statistical analysis shows that age does not have any impact in the spatial distribution of the disease. See Figure 5.3.

Figure 5.5 shows the spatial distributions for tumors larger and smaller than 10% of the whole prostate. There is SD in almost all the gland between cases with tumors larger and smaller than 10% of the whole prostate (see Figure 5.6d).

For all the cases we used Z-test for two independent proportions, the critical value is Z = 1.65. In all the cases the red color indicates SD.

The Table 5.1 shows the amount of significant difference in percentage of the whole the prostate for different cases of study. It is appreciated that values of SD for the whole prostate are quite low. Even though, there are areas of SD in the different cases being evaluated, Table 5.1 show the percentage of these regions over the whole gland is small. In Figure 5.6, the reader can appreciate that regions without SD are more common that regions with SD. Therefore, in order to get a better idea of SD in space, we propose an analysis 12 zones of the prostate. The Table 5.2 and 5.3 show the amount of significant difference by twelfth zones for different cases of study.
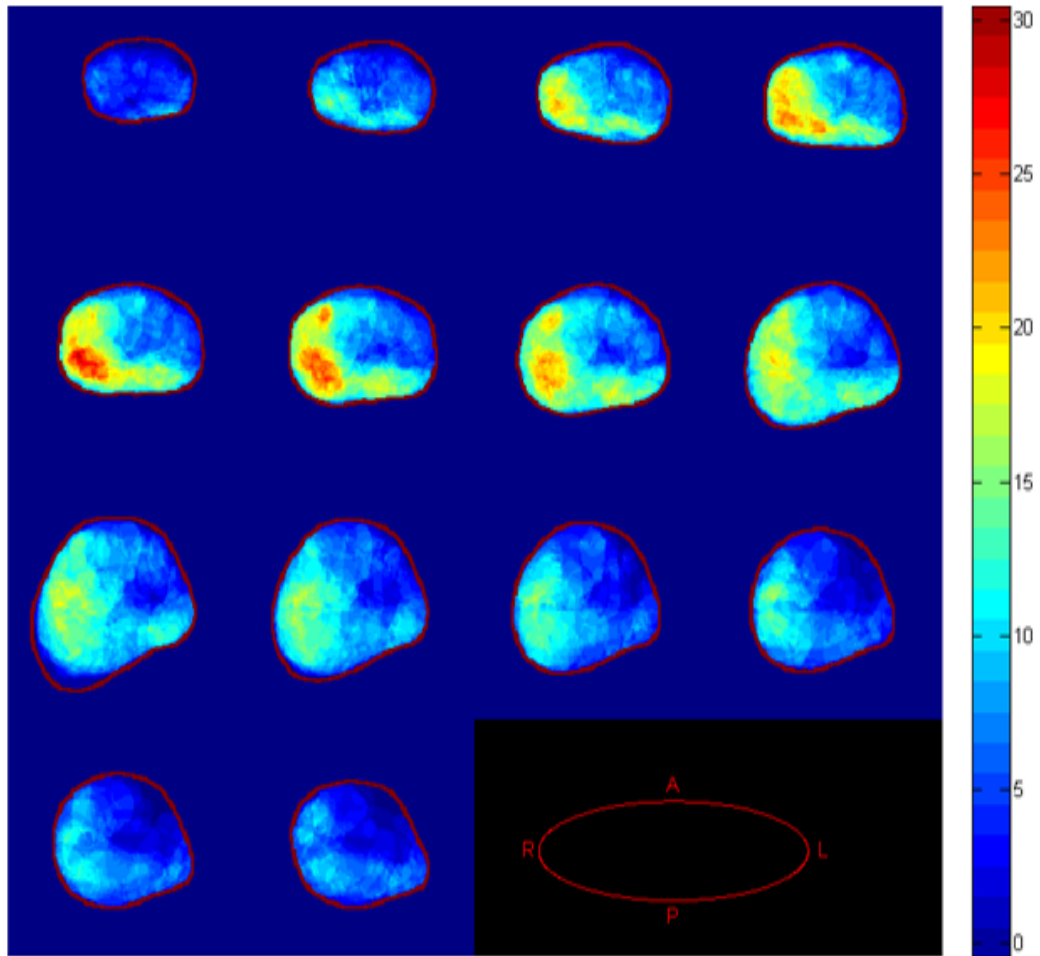
Figure 5.1: Spatial distribution of all the patients (58 patients), the color scale indicate the number of occurrences, the right zone shows to have the most level of occurrences.

Table 5.1: Significant difference in the whole prostate according to the case of study

Case of study	Significant Difference (percent of voxels within the reference atlas prostate)
PSA at time of surgery: > and ≤ 5 ng/ml	24.19%
Age: over and less than 60 years old	8.63%
Capsule penetration: positive vs negative	25.17%
Tumors size: > and ≤ 10% of the whole prostate	76.52%
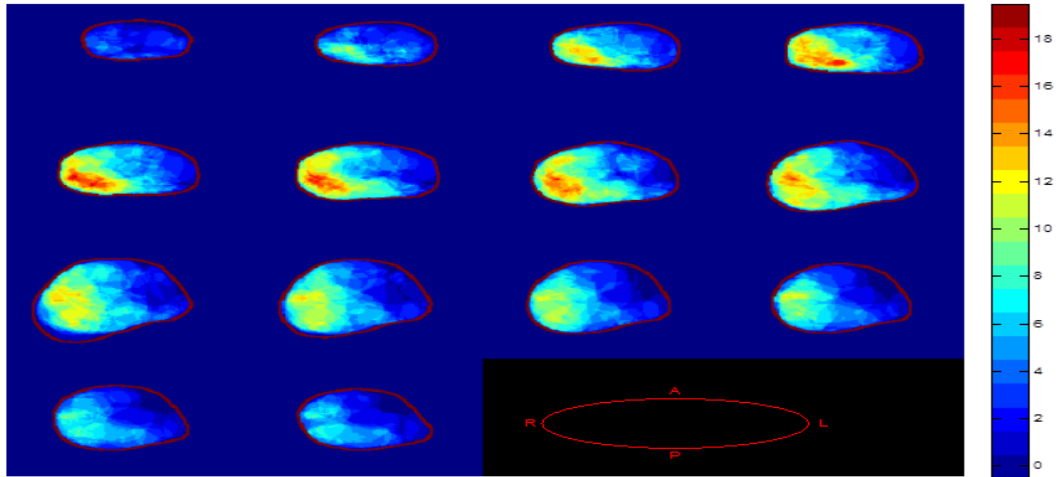
(a)
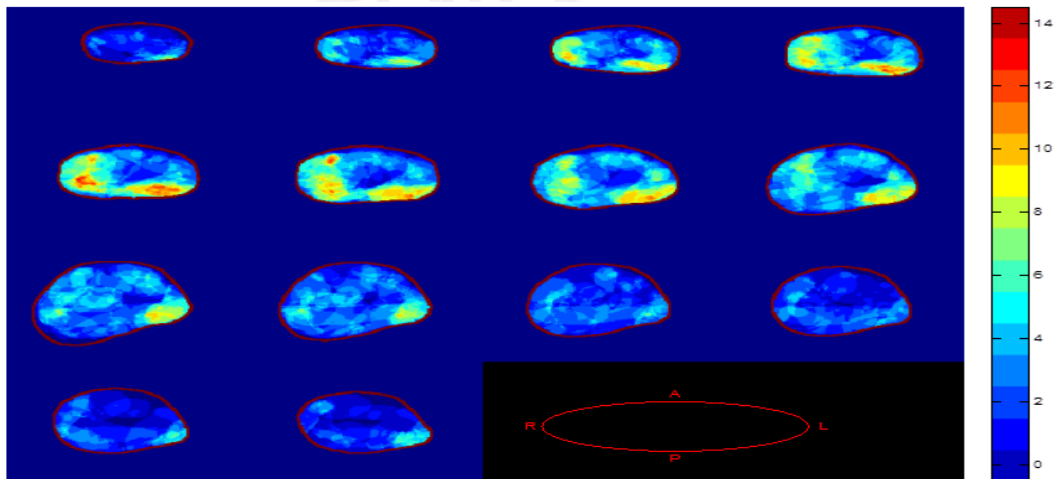
(b)
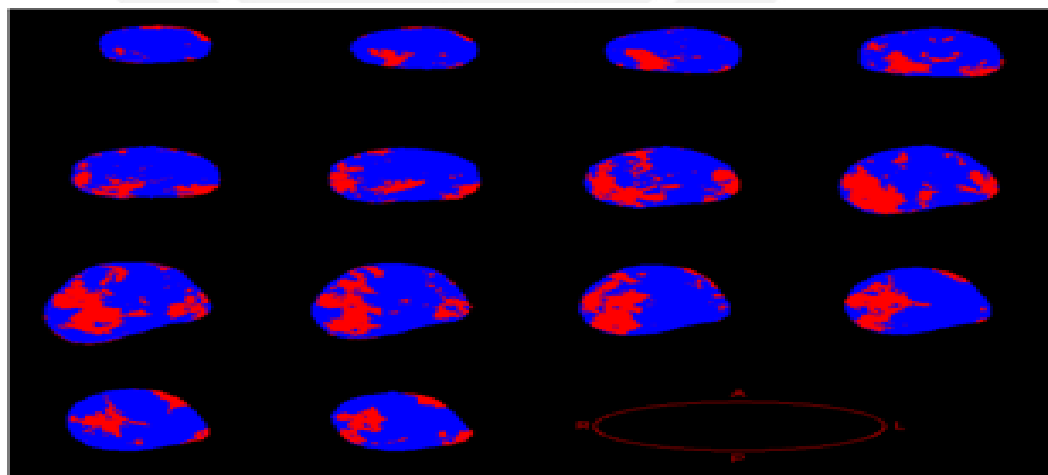
(c)

Figure 5.2: The cancer probability distribution for PSA at the time of surgery. (a) greater than 5 ng/ml / number of patients = 29/58. (b): PSA less than or equal to 5 ng/ml / number of patients = 29/58, where color scale indicate number of occurrences, the label right, left, apex and posterior is related to the patient's position. (c): significant difference (SD) using Z-test for two independent proportions. The red color indicates SD.
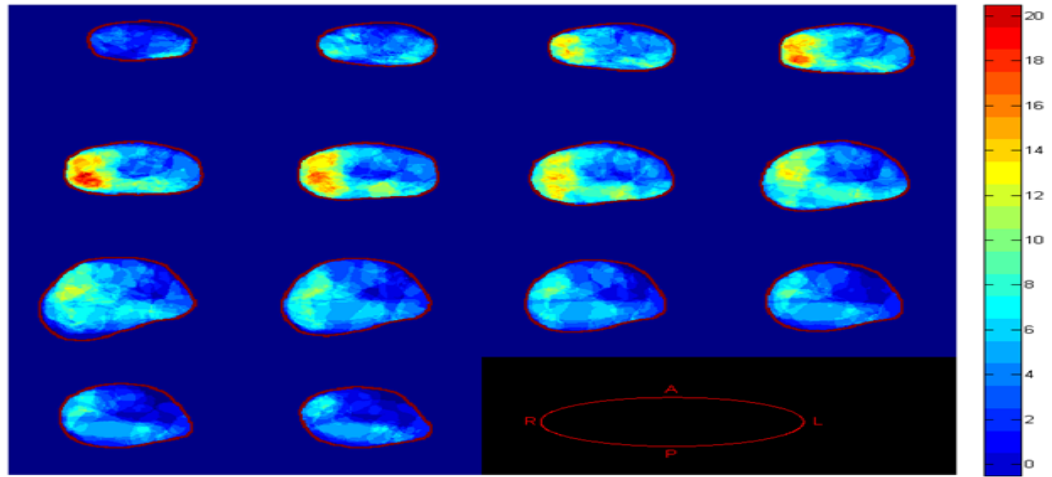
(a)
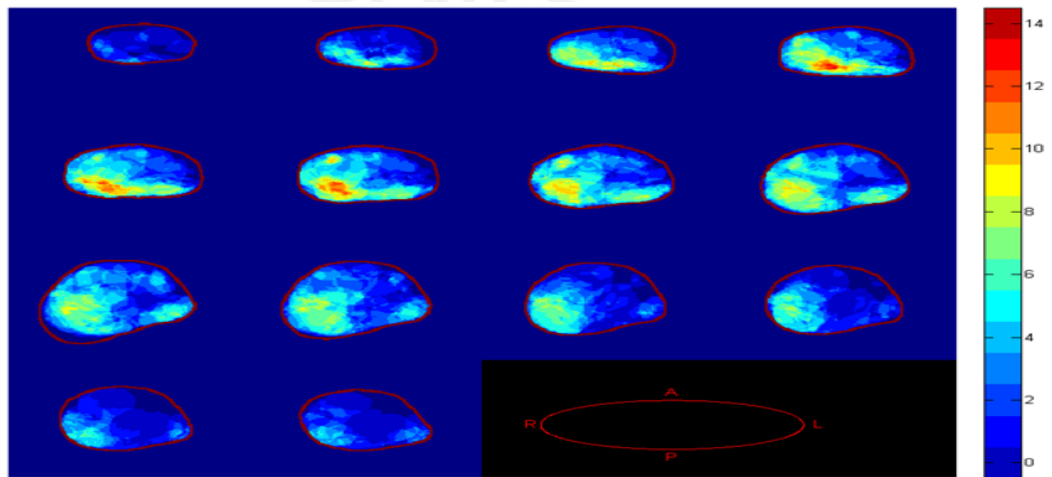
(b)
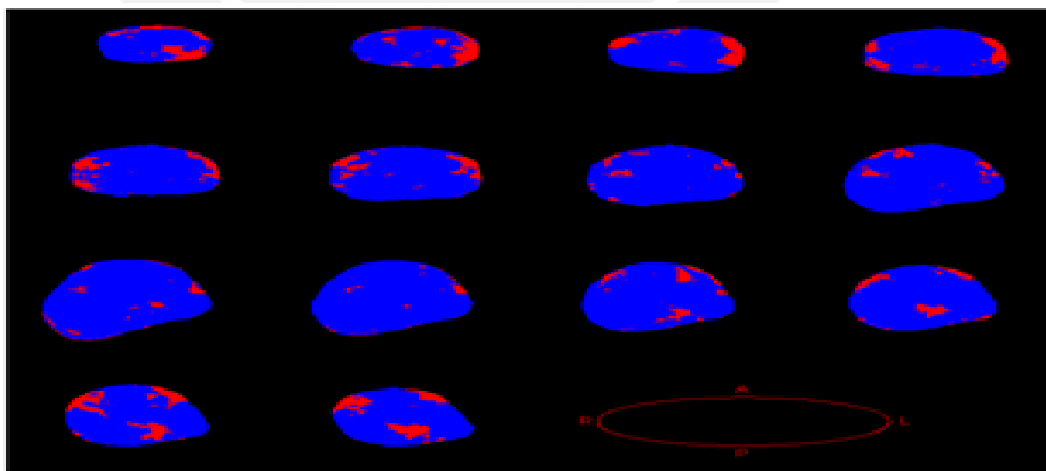
(c)

Figure 5.3: The cancer probability distribution according to the age. (a) Older than 60 years old / number of patients = 33/58. (b) Younger or equal than 60 years old/ number of patients = 25/58, where color scale indicate number of occurrences, the label right, left, apex and posterior is related to the patient's position. (c) significant difference (SD) using Z-test for two independent proportions. The red color indicates SD.
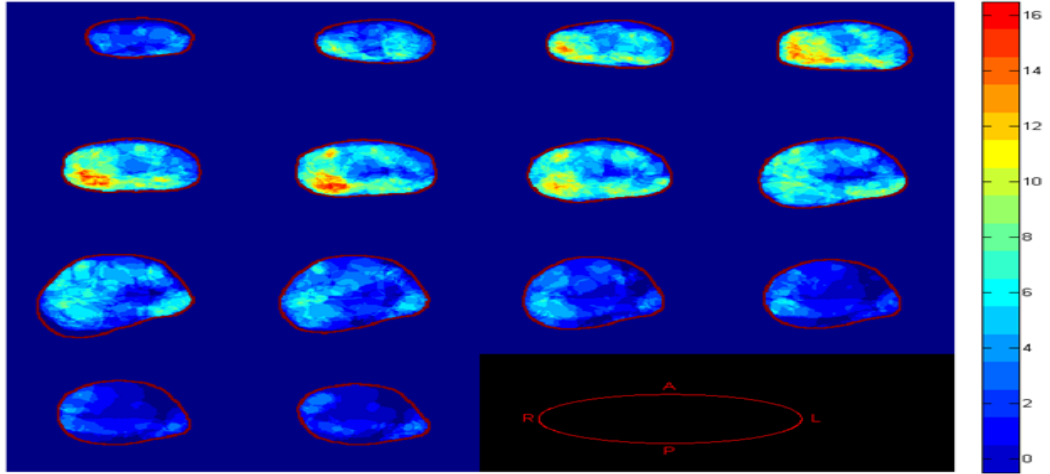
(a)
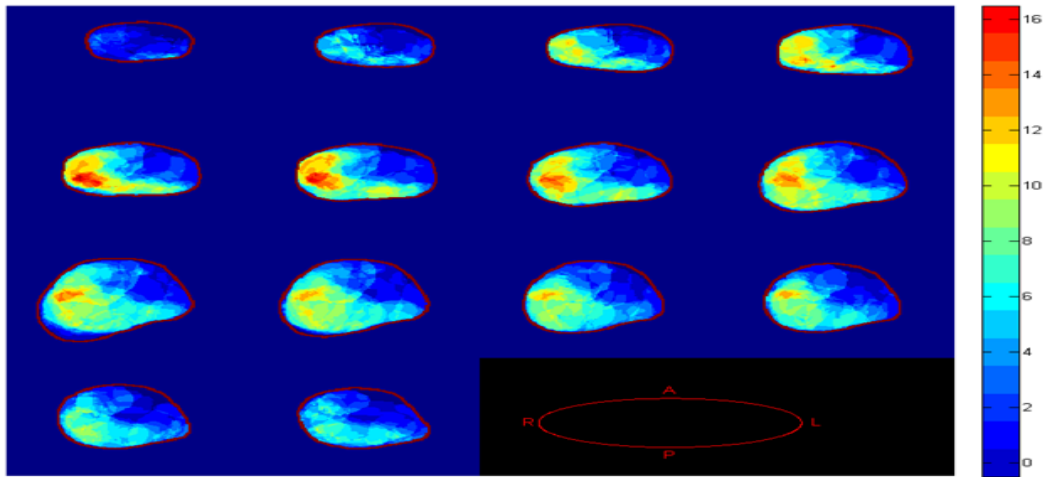
(b)
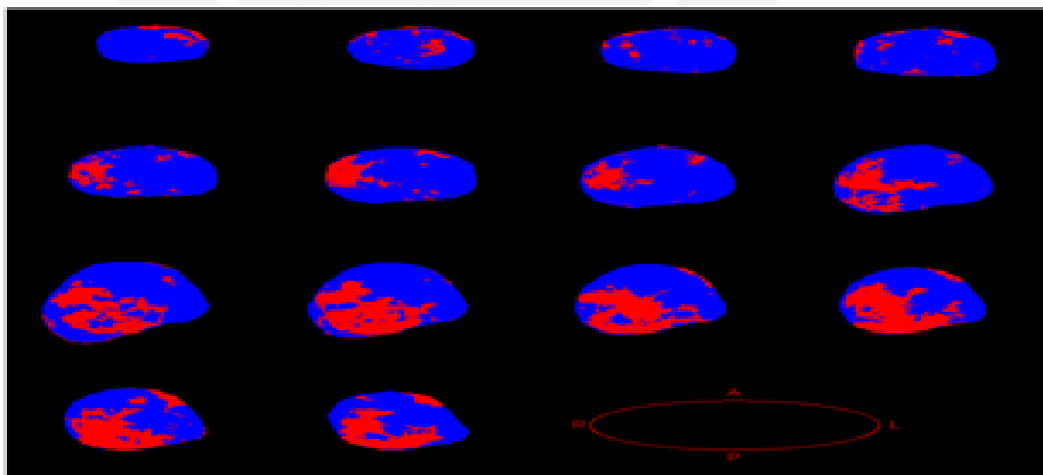
(c)

Figure 5.4: The cancer probability distribution for capsule penetration. (a) pT3 negative / number of patients = 34/58. (b) pT3 positive/ number of patients = 24/58, where color scale indicate number of occurrences, the label right, left, apex and posterior is related to the patient's position. (c) significant difference (SD) using Z-test for two independent proportions. The red color indicates SD.
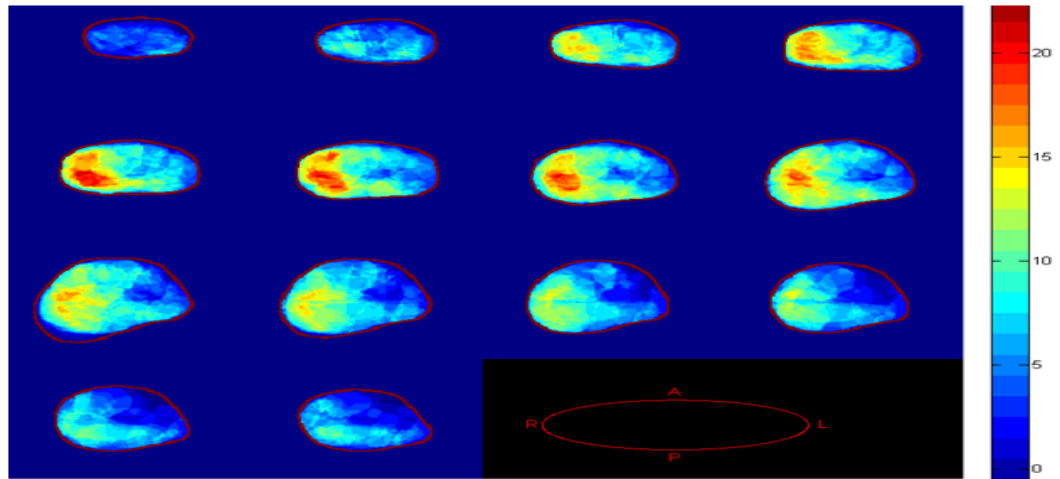
(a)
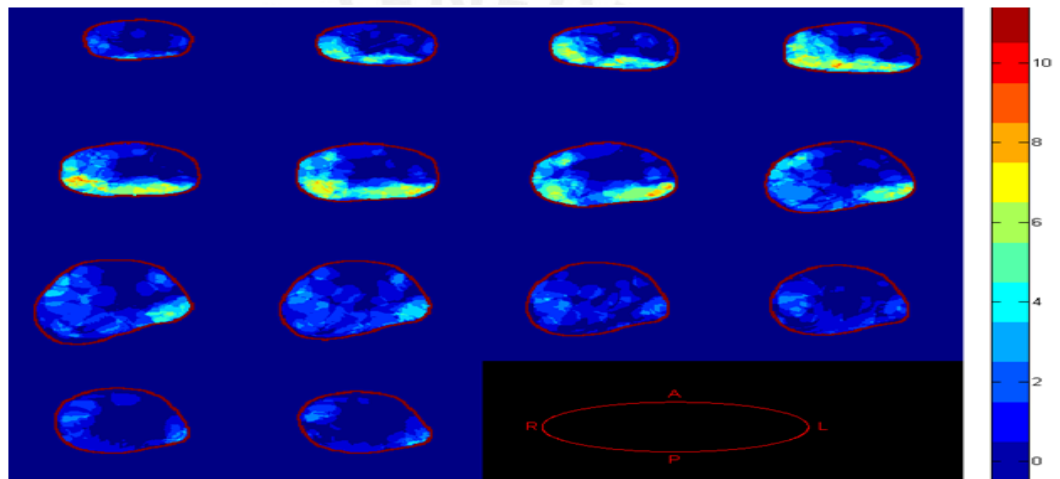
(b)
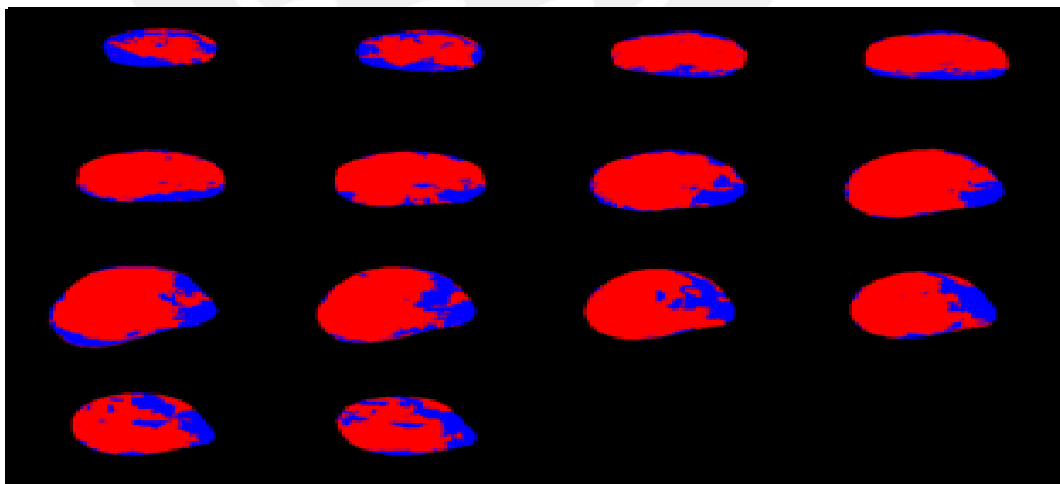
(c)

Figure 5.5: The cancer probability distribution for cancer percentage. (a) greater than 10% of whole prostate /number of patients = 28/58. (b) less than 10% of whole prostate/ number of patients = 30/58. (c) significant difference (SD) using Z-test for two independent proportions. The red color indicates SD.

(a) PSA > 5   (b) PSA ≤ 5
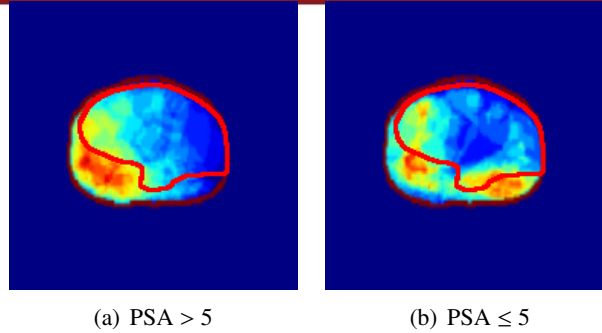
Figure 5.6: The region in red does not provide much significant difference, the amount of occurrences is very similar, so the analysis is performed by twelve zones in order to get a better idea of significant difference in space.

The data in Table 5.2 shows that PSA at the time of the surgery > and ≤ 5 ng/ml has most significant difference in the anterior and mid zone and less SD in the base. Similarly there is most SD in the anterior than in the posterior, and right than left zone. The zones with most SD are apex anterior right and mid anterior right zone, and less SD is base posterior left zone. For older and younger than 60 years old there is not any zone with a significant difference. All the zones are less than 17%.

The data in the Table 5.3 shows that for positive and negative capsule penetration the zones with SD are base and mid right, the zone with most SD is base anterior right (77.71% of SD). The zone with less SD is the left posterior. For patients with greater and less than 10 percentage of cancer, the zone with less SD is the base posterior left.

Figure 5.5 shows the two spatial distributions for patients with greater and less than 10 percentage of cancer. For patients with less than 10% of cancer, we can see that the largest amount of occurrence is given in the posterior left zone.

Table 5.2: The amount of significant difference by twelve zones for PSA > 5 vs PSA ≤ 5 (Left) and older and younger than 60 years old (Right) population. Where the first A is Apex, M is Middle, B is Base, second A is Anterior, P is Posterior, R right and L is Left of the patients.

AAR	APR	AAL	APL
50.87%	23.5%	30.12%	7.84%
MAR	MPR	MAL	MPL
50.2%	32.81%	21.78%	18.54%
BAR	BPR	BAL	BPL
34.26%	31.76%	11.18%	4.2%

PSA>5 vs PSA ≤ 5

AAR	APR	AAL	APL
3.91%	10.88%	3.09%	18%
MAR	MPR	MAL	MPL
1.88%	6.76%	1.27%	8.08%
BAR	BPR	BAL	BPL
5.74%	8.72%	17.23%	5.28%

Age>60 vs Age ≤ 60

Table 5.3: The amount of significant difference by twelve zones for positive and negative capsule penetration (left) and greater and less than 10 percentage of cancer (right) population. Where the first A is apex, M is middle, B is base, second A is anterior, P is posterior, R right and L is left of the patients.

AAR	APR	AAL	APL
8.26%	10.88%	8.49%	7.8%
MAR	MPR	MAL	MPL
40.25%	32.16%	8.89%	5.32%
BAR	BPR	BAL	BPL
77.71%	33.21%	38.38%	3.96%

Positive and negative capsule penetration

AAR	APR	AAL	APL
41.74%	78.4%	1.54%	75.23%
MAR	MPR	MAL	MPL
84.68%	98.26%	40.89%	69.23%
BAR	BPR	BAL	BPL
92.06%	88.53%	62.69%	28.75%

Greater and less than 10% of cancer

Chapter 6

Discussion and Conclusions

Probabilistic maps are used to investigate where it is more likely to develop cancer within the prostate gland. The goal of this thesis is to develop a computational tool which extends the use of probabilistic maps for a statistical analysis of prostate cancer between different populations in relation to its clinical parameters: PSA, capsule penetration, age of the patients and cancer percentage. This analysis provides spatial significant differences between maps which would increase our understanding of this disease in relation to its clinical parameters. This tool would help create a starting point for future works to comprehend the relationship between tumor distributions and different surrogate markers. Therefore, this study could have a significant impact in academic research.

Several computer-assisted approaches [12, 14, 17, 18, 19, 20, 21, 22, 24, 27, 34, 35] developed in this field have been focused on the maximization of the probability that biopsy needles intersect with the tumor and the improvement of cancer detection without considering other clinical parameters. This tool can estimate spatial distribution of the cancer using clinical parameters which have a significant impact on clinical research, with the addition of clinical parameters is possible to have a probabilistic map customized by patient.

Histopathological images were used to create the spatial distribution of prostate cancer. Pathology experts outlined the location of the cancer on the image. The distance between the cuts was between $4mm$ and $7mm$, so it required an interpolation step in order to have an isotropic volume. However in the specialized literature [12, 14, 17, 18, 19, 20, 21, 22, 24, 27, 34, 35] a criterion has not yet been established for the reconstruction of the tumor, since it can grow in any direction and orientation (see Figure 3.11). In this work, two decision rules were introduced in order to avoid ambiguities in the reconstruction of the tumor (see chapter 3, section 4).

The database has been formed by glands after whole prostatectomy with a cancer diagnosis. Consequently, the database has not got a healthy prostate, and the probabilistic model has some deformation because of the presence of a tumors. An expert pathologist manually selected one prostate from the database with an average size and shape to be the atlas model. This process is similar to other reported studies [18, 19, 22, 39], and does not

TESIS PUCP

CHAPTER 6. DISCUSSION AND CONCLUSIONS

PONTIFICIA
UNIVERSIDAD
CATÓLICA
DEL PERÚ
41

affect the statistical analysis used since the same prostate is used for the registration step.

Most of the statistical analyses are based on the hypothesis about two independent population medians (The Mann-Whitney U test and Kolmogorov-Smirnov test for two independent samples) which perform a comprehensive analysis of the distributions indicating the similarity between populations. However these analyses do not give spatial difference between two populations. The Z-test for two independent proportions was proposed in order to determine the most significant difference voxel by voxel. We analyze differences in distribution between two populations where each population has a common pathological variable.

These analyzes give an overall comparison of the distribution between two populations without knowledge of spatial location. The goal in this thesis is to develop a spatial analysis in order to determine the most significant difference in a voxel by voxel basis.

During the development of this thesis, a number of questions have appeared based on the results. For example, why is prostate cancer more likely to appear to the right of patient? Previous studies on 3D spatial distribution of prostate cancer [15, 16, 17, 18, 19, 20] have shown agreement with the results obtained in this work. The area with the highest number of occurrences is the right zone, more accurate in the right posterior peripheral zone near to the base of the prostate. This result confirms the medical knowledge gained by experience; however an explanation for this has not yet been given in the literature.

Other question is whether there is any difference in the cancer location between young and old patients? According to the results there is no difference in the spatial distribution of cancer among these groups of people. This analysis should be completed with other clinical parameters such PSA in order to understand the aggressiveness of cancer in young people. A larger database is required to perform a multivariate analysis.

Also is important to answer, where is more likely to appear cancer in its early stages? i.e. when the tumor appear where is it more likely to be located? Based on the results obtained, prostate cancer is more likely to appear in the posterior part (cancer percentage less than 10% of the whole prostate, see Figure 5.5) and the area closest to the rectum, and then it spreads to the rest of the gland. This result emphasizes the value of DRE in the early stages because it is more probable that the cancer starts in the area to which the doctor has access.

One of the most important questions to the scientific community both clinical and academic is the understanding of PSA as a marker and determines whether the value of PSA cutoff is more appropriate. In the USA and Peru, the PSA value of 4 ng/ml has become widely used as a decision limit to identify prostate cancer in its early stages, but this value does not mean that the disease is advanced enough to extract the prostate gland. The prob-

ability of finding prostate cancer with a serum PSA of 4 *ng/ml* is about 20% [45]. In our database, the total number of patients that have PSA less than 4 *ng/ml* is 14 of 58 (24.14%) so, it requires a greater number of patients to have a significant sample of men with PSA less than 4 *ng/ml*.

The value of 5 *ng/ml* was used as cutoff to develop two spatial distributions to compare two populations and find significant differences. The value of 5 *ng/ml* was chosen because of the PSA concentrations in serum increase with age [66] and the average age of our database is 59.8 ± 5.472 ranging from 48.5 to 72.8 years old. According to our results prostate cancer has a significant difference in the right zone of the prostate in patients with PSA over than and less than 5 *ng/ml*.

Currently, there is no consensus on the selection of the cutoff [67]. A low PSA cutoff $(0.2 - 2\ ng/ml)$ can cause unnecessary treatment which results in an overmedication affecting the quality of life on the patients. On the other hand, high PSA cutoff value $(> 7ng/ml)$ can cause the treatment is not longer enough to remove the cancer. The PSA cutoff value should be studied in conjunction with other pathological variables as age and prostate volume. This tool could be used to set various PSA cutoffs and determine if there is a critical value of PSA and set this cutoff for future research in order to understand the disease.

An analysis of 12 zones of the prostate was proposed for a better understanding of the spatial distribution of the tumor. These zones are chosen according clinical conventions, and the significant differences in each zone are calculated. The results from the statistical analysis show that the anterior right zones have more significant difference $(> 34\%)$ for PSA greater than 5 *ng/ml* against PSA less than 5 *ng/ml*; there is also a significantly higher cancer distribution (77.71%) in the base anterior right zone for Positive and negative capsule penetration.

An analysis by zones based on the prostate anatomical region: Transition Zone, Peripheral zone, Central Zone and Fibro muscular stroma should be more clinically relevant than an overall analysis of the whole prostate. The developed tool could provide this analysis using a previously segmented gland by an expert radiologist to divide the regions.

A limitation of this study is the small database: 58 prostate specimens are not sufficient to represent correctly the spatial distributions of the cancer. This amount of samples limits our ability to perform a multivariate analysis. A multivariate analysis would allow us to find and study relationships between populations with more than one requirement. The tool developed in this thesis can make the analysis with more the one clinical parameter, e. g. the analysis for men older than 80 years old and with PSA greater than 5 *ng/ml*.

A larger database is needed to improve statistical validity of the test. A solution would be multi-institutional studies and data sharing processes; a larger sample size could give

a more realist distribution independently of the acquisition process with less bias. We are planning to validate our result and increase the population using the database of the Section of Biomedical Image Analysis (SBIA), University of Pennsylvania, Philadelphia, USA.

To summarize, the main contributions of this work are the image processing methodology to develop the spatial distribution from a database of whole mount histology sections, and the statistical analysis to compare two spatial distributions based on differences of proportions.

Bibliography

[1] Mayo Clinic, "Prostate cancer, transrectal biopsy of the prostate.," Tech. Rep., Mayo Foundation for Medical education and research., 8 2012.

[2] Betrouni N., Iancu A., Puech P., Mordon S., and Makni N., "Prostatlas: a digital morphologic atlas of the prostate.," *European Journal of Radiology*, vol. 81, no. 9, pp. 1969 – 1975, 2012.

[3] Taylor L. S., Porter B. C., Nadasdy G., di SantAgnese P. A., Pasternack D., Wu Z., Baggs R. B., Rubens D. J., and Parker K. J., "Three-dimensional registration of prostate images from histology and ultrasound.," *Ultrasound in Medicine & Biology*, vol. 30, no. 2, pp. 161 – 168, 2004.

[4] Zhu Y., Williams S., and Zwiggelaar R., "Computer technology in detection and staging of prostate carcinoma: A review.," *Medical Image Analysis*, vol. 10, no. 2, pp. 178 – 199, 2006.

[5] Sobin L. H., Gospodarowicz M. K., and Wittekind Ch., *TNM classification of Malignant tumours.*, Wiley-Blackwell, seventh edition, 2009.

[6] Stott P., "The prostate : small gland, big problem.," *International Journal of Clinical Practice*, vol. 58, no. 6, pp. 647–647, 2004.

[7] Ablin R. J. and Mason M. D., *Metastasis of prostate cancer.*, vol. 10, Springer; 1 edition, 2007.

[8] Oficina General de Planteamiento y Presupuesto, "Instituto nacional de enfermedades neoplsicas organismo publico ejecutor: Plan operativo institucional 2011.," Tech. Rep., Instituto Nacional de Enfermedades Neoplsicas, 2011.

[9] Ferlay J, Shin HR, Bray F, Forman D, Mathers C, and Parkin DM., "Globocan 2008 v1.2, cancer incidence and mortality worldwide: Iarc cancerbase no. 10 [internet].lyon, france: International agency for research on cancer; 2010.," may 2008.

[10] Jewett H. J., "Significance of the palpable prostatic nodule.," *Journal of the American Medical Association*, vol. 160, no. 10, pp. 838–839, 1956.

[11] Schroder F. H., Kruger A. B., Rietbergen J., Kranse R., Maas P., Beemsterboer P., and Hoedemaeker R., "Evaluation of the digital rectal examination as a screening

test for prostate cancer.," *JNCI Journal of the National Cancer Institute*, vol. 90, pp. 1817–1823, 1998.

[12] Tang J., Yang J. C., Li Y., Li J., and Shi H., "Peripheral zone hypoechoic lesions of the prostate.," *Journal of Ultrasound in Medicine*, vol. 26, no. 12, pp. 1671–1679, 2007.

[13] Flanigan R. C.and Catalona W. J., Richie J. P., Ahmann F. R., Hudson M. A., Scardino P. T., deKernion J. B., Ratliff T. L., Kavoussi L. R., and Dalkin B. L., "Accuracy of digital rectal examination and transrectal ultrasonography in localizing prostate cancer.," *The Journal of urology*, vol. 152, no. 5, pp. 1506–1509, 1994.

[14] Bauer J. J., Zeng J., Weir J., Zhang W., Sesterhenn I. A., Connelly R. R., Mun S. K., and Moul J. W., "Three-dimensional computer-simulated prostate models: lateral prostate biopsies increase the detection rate of prostate cancer.," *Urology*, vol. 53, no. 5, pp. 961 – 967, 1999.

[15] Bauer J. J., Zeng J., Zhang W., McLeod D. G., Sesterhenn I. A., Connelly R. R., Mun S. K., and Moul J. W., "3-d computer visualization and interactive prostate biopsy simulation leads to an improved systematic technique for the detection of prostate cancer: clinical correlation.," *Studies In Health Technology And Informatics*, vol. 70, pp. 20–25, 2000.

[16] Bauer J. J., Zeng J., Zhang W., McLeod D. G., Sesterhenn I. A., Connelly R. R., Mun S. K., and Moul J. W., "Lateral biopsies added to the traditional sextant prostate biopsy pattern increases the detection rate of prostate cancer.," *Prostate cancer and prostatic diseases*, vol. 3, no. 1, pp. 43–46, 2000.

[17] Zeng J., Bauer J., Zhang W., Sesterhenn I., Connelly R., Lynch J., Moul J., and Mun S. K., "Prostate biopsy protocols: 3d visualization-based evaluation and clinical correlation.," *Computer Aided Surgery*, vol. 6, no. 1, pp. 14–21, 2001.

[18] Zeng J., Bauer J. J., and Mun S. K., "Modeling and mapping of prostate cancer.," *Computers & Graphics*, vol. 24, no. 5, pp. 683 – 694, 2000, Dynamic Medical Visualization (special topic).

[19] Zeng J., Bauer J., Sofer A., Yao X., Opell B., Zhang W., Sesterhenn I., Moul J., Lynch J., and Mun S., "Distribution of prostate cancer for optimized biopsy protocols.," in *Medical Image Computing and Computer-Assisted Intervention MICCAI 2000*, Scott Delp, Anthony DiGoia, and Branislav Jaramaz, Eds., vol. 1935 of *Lecture Notes in Computer Science*, pp. 141–177. Springer Berlin / Heidelberg, 2000.

[20] Shen D., Lao Z., Zeng J., Herskovits E., Fichtinger G., and Davatzikos C., "A statistical atlas of prostate cancer for optimal biopsy.," in *Medical Image Computing and Computer-Assisted Intervention MICCAI 2001*, Wiro Niessen and Max Viergever, Eds. 2001, vol. 2208 of *Lecture Notes in Computer Science*, pp. 416–424, Springer Berlin / Heidelberg.

[21] Shen D., Lao Z., Zeng J., Herskovits E. H., Fichtinger G., and Davatzikos C., "Statistically optimized biopsy strategy for the diagnosis of prostate cancer.," in *Computer-Based Medical Systems, 2001. CBMS 2001. Proceedings. 14th IEEE Symposium on*, 2001, pp. 433 –438.

[22] Opell M. B., Zeng J., Bauer J. J., Connelly R. R., Zhang W., Sesterhenn I. A., Mun S. K., Moul J. W., and Lynch J. H., "Investigating the distribution of prostate cancer using three-dimensional computer simulation.," *Prostate Cancer and Prostatic Diseases*, vol. 5, no. 3, pp. 204–8, 2002.

[23] Sofer A., Zeng J., and Mun S. K., "Optimal biopsy protocols for prostate cancer.," *Annals of Operations Research*, vol. 119, pp. 63–74, 2003.

[24] Shen D., Lao Z., Zeng J., Zhang W., Sesterhenn I. A., Sun L., Moul J. W., Herskovits E. H., Fichtinger G., and Davatzikos C., "Optimized prostate biopsy via a statistical atlas of cancer spatial distribution.," *Medical Image Analysis*, vol. 8, no. 2, pp. 139 – 150, 2004.

[25] Zeng J., Kaplan C., Bauer J., Zhang W., Sesterhenn I., Moul J., and Mun S. K., "Visualization and evaluation of prostate needle biopsy.," in *The First International Conference on Medical Image Computing and Computer-Assisted Intervention*, WilliamM. Wells, Alan Colchester, and Scott Delp, Eds., vol. 1496 of *Lecture Notes in Computer Science*, pp. 285–292. Springer Berlin Heidelberg, 1998.

[26] Chen M. E., Troncoso P., Johnston D., Tang K., and Babaian R. J., "Optimization of prostate biopsy strategy using computer based analysis.," *The Journal of urology*, vol. 158, no. 6, pp. 2168–2175, 1997.

[27] Chen M. E., Troncoso P., Tang K., Babaian R. J., and Johnston D., "Comparison of prostate biopsy schemes by computer simulation.," *Urology*, vol. 53, no. 5, pp. 951 – 960, 1999.

[28] Chen M. E., Troncoso P., Johnston D., Tang K., and Babaian R. J., "Prostate cancer detection: relationship to prostate size.," *Urology*, vol. 53, no. 4, pp. 764 – 768, 1999.

[29] Babaian R. J., Toi A., Kamoi K., Troncoso P., Sweet J., Evans R., Johnston D., and Chen M., "A comparative analysis of sextant and an extended 11-core multisite directed biopsy strategy.," *The Journal of Urology*, vol. 163, no. 1, pp. 152 – 157, 2000.

[30] Loch T. and Chen M. E., "Computer simulation of prostate biopsies.," *European urology*, vol. 1, pp. 47 – 51, 2002.

[31] Daneshgari F., Taylor G. D., Miller G. J., and Crawford E. D., "Computer simulation of the probability of detecting low volume carcinoma of the prostate with six random systematic core biopsies.," *Urology*, vol. 45, no. 4, pp. 604 – 609, 1995.

[32] Crawford E. D., Hirano D., Werahera P. N., Lucia M. S., Deantoni E. P., Daneshgari F., Brawn P. N., Speights V. O., Stewart J. S., and Miller G. J., "Computer modeling

of prostate biopsy: Tumor size and location-not clinical significance-determine cancer detection.," *The Journal of Urology*, vol. 159, no. 4, pp. 1260 – 1264, 1998.

[33] Kawata N., Miller G. J., Crawford E. D., Torkko K. C., Stewart J. S., Lucia M. S., Miller H. L., Hirano D., and Werahera P. N., "Laterally directed biopsies detect more clinically threatening prostate cancer: Computer simulated results.," *The Prostate*, vol. 57, no. 2, pp. 118–128, 2003.

[34] Loughlin M., Carlbom I., Busch C., Douglas T., Egevad L., Frimmel H., Norberg M., Sesterhenn I., and Frogge J. M., "Three-dimensional modeling of biopsy protocols for localized prostate cancer.," *Computerized Medical Imaging and Graphics*, vol. 22, no. 3, pp. 229 – 238, 1998.

[35] Frimmel H., Egevad L., Bengtsson E., and Busch C., "Modeling prostate cancer distributions.," *Urology*, vol. 54, no. 6, pp. 1028 – 1034, 1999.

[36] Egevad L., Frimmel H., Mattson S., Bengtsson E., and Busch C., "Biopsy protocol stability in a three-dimensional model of prostate cancer: changes in cancer yield after adjustment of biopsy positions.," *Urology*, vol. 54, no. 5, pp. 862 – 868, 1999.

[37] Egevad L., Frimmel H., Norberg M., Mattson S., Carlbom I., Bengtsson E., and Busch C., "Three-dimensional computer reconstruction of prostate cancer from radical prostatectomy specimens: evaluation of the model by core biopsy simulation.," *Urology*, vol. 53, no. 1, pp. 192 – 198, 1999.

[38] Xuan J., Wang Y., Sesterhenn I., Moul J., and Mun S., "3-d model supported prostate biopsy simulation and evaluation.," in *Medical Image Computing and Computer-Assisted Intervention MICCAI 1998*, William Wells, Alan Colchester, and Scott Delp, Eds., vol. 1496 of *Lecture Notes in Computer Science*, pp. 358–367. Springer Berlin / Heidelberg, 1998.

[39] Shen D. and Davatzikos C., "An adaptive-focus deformable model using statistical and geometric information.," *Pattern Analysis and Machine Intelligence, IEEE Transactions on*, vol. 22, no. 8, pp. 906 –913, aug 2000.

[40] Shen D., Herskovits E. H., and Davatzikos C., "An adaptive-focus statistical shape model for segmentation and shape modeling of 3-d brain structures.," *Medical Imaging, IEEE Transactions on*, vol. 20, no. 4, pp. 257 –270, april 2001.

[41] Ou Y., Shen D., Zeng J., Sun L., Moul J., and Davatzikos C., "Sampling the spatial patterns of cancer: Optimized biopsy procedures for estimating prostate cancer volume and gleason score.," *Medical Image Analysis*, vol. 13, no. 4, pp. 609 – 620, 2009.

[42] McCormack M., "Canadian family physician.," *Prostate Cancer New serum tumor marker for monitoring patients*, vol. 38, pp. 1438–1440, june 1992.

[43] Brawer M. K., Chetner M. P., Beatie J., Buchner D. M., Vessella R. L., and Lange P. H., "Screening for prostatic carcinoma with prostate specific antigen.," *The Journal of urology*, vol. 147, pp. 841–5, 1992.

[44] Catalona W. J., Smith D. S., Ratliff T. L., and Basler J. W., "Detection of organ-confined prostate cancer is increased through prostate-specific antigen-based screening.," *JAMA : the journal of the American Medical Association*, vol. 270, pp. 948–54, 1993.

[45] Crawford E. D., DeAntoni E. P., Etzioni R., Schaefer V. C., Olson R. M., Ross C. A., and The Prostate Cancer Education Council., "Serum prostate-specific antigen and digital rectal examination for early detection of prostate cancer in a national community-based program.," *Urology*, vol. 47, no. 6, pp. 863 – 869, 1996.

[46] Mettlin C., Lee F., Drago J., and Murphy G. P., "The american cancer society national prostate cancer detection project: findings on the detection of early prostate cancer in 2425 men.," *Cancer*, vol. 67, no. 12, pp. 2949–58, 1991.

[47] Brawer M. K. and Kirby R., *Prostate Specific Antigen.*, Marcel Dekker, 2001.

[48] Li-Ming Su MD., *Early Diagnosis and Treatment of Cancer Series: Prostate Cancer.*, Saunders; 1 Har/Psc edition, November 2009.

[49] Egevad L., Engstrom K., and Busch C., "A new method for handling radical prosta-tectomies enabling fresh tissue harvesting, whole mount sections, and landmarks for alignment of sections.," *Journal Urology Pathology,*, vol. 9, pp. 1728, 1998.

[50] George Wolberg, *Digital Image Warping.*, IEEE Computer Society Press, 1990.

[51] Beier T. and Neely S., "Feature-based image metamorphosis.," *Computer graphics and interactive techniques*, vol. 2, pp. 35–42, 1992.

[52] Rafael C. Gonzalez and Richard E. Woods, *Digital Image Processing (3rd Edition).*, Prentice-Hall, Inc., Upper Saddle River, NJ, USA, 2006.

[53] Otsu N., "A threshold selection method from gray-level histograms," *Systems, Man and Cybernetics, IEEE Transactions on*, vol. 9, no. 1, pp. 62 –66, jan. 1979.

[54] Ladak H. M., Mao F., Wang Y., Downey D. B., Steinman D. A., and Fenster A., "Prostate boundary segmentation from 2d ultrasound images.," *Medical Physics*, vol. 27, no. 8, pp. 1777–88, 2000.

[55] Lobregt S. and Viergever M. A., "A discrete dynamic contour model.," *Medical Imaging, IEEE Transactions on*, vol. 14, no. 1, pp. 12 –24, mar 1995.

[56] Kels S. and Dyn N., "Reconstruction of 3d objects from 2d cross-sections with the 4-point subdivision scheme adapted to sets.," *Computers & Graphics*, vol. 35, no. 3, pp. 741 – 746, 2011.

[57] Albu A. B., Beugeling T., and Laurendeau D., "A morphology-based approach for interslice interpolation of anatomical slices from volumetric images.," *Biomedical Engineering, IEEE Transactions on*, vol. 55, no. 8, pp. 2022–2038, 2008.

[58] Csebfalvi B., Neumann L., Kanitsar A., and Groller E., "Smooth shape-based interpolation using the conjugate gradient method.," *Proceedings of vision, modeling, and visualization.*, p. 12330, 2002.

[59] Lin W. C., Liang C. C., and Chen C. T., "Dynamic elastic interpolation for 3d medical image reconstruction from serial cross sections.," *Medical Imaging, IEEE Transactions on*, vol. 7, no. 3, pp. 225 –232, sep 1988.

[60] Raya S. P. and Udupa J. K., "Shape-based interpolation of multidimensional objects.," *Medical Imaging, IEEE Transactions on*, vol. 9, no. 1, pp. 32 –42, mar 1990.

[61] Herman G.T., Zheng J., and Bucholtz C. A., "Shape-based interpolation.," *Computer Graphics and Applications, IEEE*, vol. 12, no. 3, pp. 69 –79, may 1992.

[62] Lee T. Y. and Wang W. H., "Morphology-based three-dimensional interpolation.," *Medical Imaging, IEEE Transactions on*, vol. 19, no. 7, pp. 711 –721, july 2000.

[63] McNeal J. E., Redwine E. A., and Stamey T. A., "Zonal distribution of prostatic adenocarcinoma. correlation with histologic.," *The American journal of surgical pathology*, vol. 12, no. 12, pp. 897–906, 1988.

[64] Erbersdobler A., Huhle S., Palisaar J., Graefen M., Hammerer P., Noldus J., and Huland H., "Pathological and clinical characteristics of large prostate cancers predominantly located in the transition zone.," *Prostate Cancer Prostatic Dis*, vol. 5, pp. 279–84, 2002.

[65] Terry S. Yoo., *Insight into images: principles and practice for segmentation, registration, and image analysis.*, AK Peters, first edition, 2004.

[66] Castaneda B., Wu S., Hoyt K., Baxter L., Yao J., Pasternack D., Strang J., Rubens D. J., and Parker K.J., "Application of nonrigid registration to validate detection of prostate cancer using threedimensional sonoelastography.," *Proceedings of the Seventh International Conference on the Ultrasonic Measurement and Imaging of Tissue Elasticity*, p. 62, 2008.

[67] David J.Sheskin, *Parametric And Nonparametric Statistical Procedures Second Edition.*, Chapman & Hall/Crc, 2000.